Oecologia (2018) 187:1053–1075
https://doi.org/10.1007/s00442-018-4189-0

SPECIAL TOPIC

Distinctions in heterotrophic and autotrophic-based metabolism as recorded in the hydrogen and carbon isotope ratios of *normal* alkanes

Brett J. Tipple[1,2] **· James R. Ehleringer**[1,2]

Received: 22 July 2017 / Accepted: 5 June 2018 / Published online: 28 June 2018

Abstract

The hydrogen isotope values of *n*-alkanes ($\delta^2H_{n\text{-alkane}}$) reflect a plant's water source and water relations, while the carbon isotope values ($\delta^{13}C_{n\text{-alkane}}$) relate to a plant's carbon metabolism and response to environmental conditions. However, the isotopic dynamics of the transition from heterotrophic to autotrophic metabolism during foliar development on $\delta^2H_{n\text{-alkane}}$ and $\delta^{13}C_{n\text{-alkane}}$ remain unclear. Here, we monitored $\delta^2H_{n\text{-alkane}}$ and $\delta^{13}C_{n\text{-alkane}}$ across a growing season from *Betula occidentalis*, *Populus angustifolia*, and *Acer negundo*. In addition, we compiled δ^2H values of atmospheric vapor, leaf water, xylem water, and stream water as well as $\delta^{13}C$ values of bulk leaf tissue ($\delta^{13}C_{bulk}$). We found $\delta^2H_{n\text{-alkane}}$ and $\delta^{13}C_{n\text{-alkane}}$ varied with leaf development and indicated that the majority of wax development occurred during the initial growing season. The patterns in $\delta^2H_{n\text{-alkane}}$ were broadly consistent between species and with previous studies; however, each species had a unique final $\delta^2H_{n\text{-alkane}}$ value. The $\delta^{13}C_{bulk}$ for all species demonstrated a characteristic ^{13}C-enrichment during the initial growing season, followed by ^{13}C-depletion, while $\delta^{13}C_{n\text{-alkane}}$ did not exhibit a consistent trend between the species. These $\delta^{13}C$ data suggested a decoupling of the isotopic inputs between *n*-alkanes and photosynthetic leaf tissue. When coupled with $\delta^2H_{n\text{-alkane}}$, these data suggested that the precursor compounds utilized in initial production of *n*-alkanes might be variable and possibly indicated that the stored precursors used for initial leaf tissue and wax production originated from different sources. Nonetheless, these data indicated that the isotopic signatures of *n*-alkanes relate to a mixture of precursors, but only during a distinct period of leaf ontogeny.

Keywords Leaf wax · Cuticle · Stable isotope · Compound-specific isotope analysis · Ecophysiology

Introduction

Stable isotope analyses of plant tissues and compounds have become an indispensable tool to understand plant physiology, ecology, photosynthetic pathway, and growth conditions (e.g., Berke et al. 2015; Dawson and Ehleringer 1991, 1993; Ehleringer et al. 1986; Farquhar et al. 1989; Feakins and Sessions 2010a; Flanagan et al. 1991; Gessler et al. 2009; Helliker and Ehleringer 2002; Kahmen et al. 2011; Roden and Ehleringer 1999; Rundel et al. 1989; Sparks and Ehleringer 1997; Tipple and Pagani 2013; Zimmerman and Ehleringer 1990). Measurement of stable isotopes from historical and ancient plant materials, such as tree-ring cellulose, ancient soil organic matter, and sedimentary leaf wax lipids, is regularly used to reconstruct past ecologic and climatic conditions (Alstad et al. 2008; Cerling et al. 1994; Cook et al. 2010; Freeman and Colarusso 2001; Griffin and Anchukaitis 2014; Leavitt et al. 2011; McCarroll and Loader 2004; Smith et al. 2007; Treydte et al. 2009, among others). Recent advancements in compound-specific isotope ratio mass spectrometry and extraction methods have allowed for increased analysis throughput and development of higher resolution hydrogen (δ^2H) and/or carbon

Communicated by Joy K. Ward.

Electronic supplementary material The online version of this article (https://doi.org/10.1007/s00442-018-4189-0) contains supplementary material, which is available to authorized users.

✉ Brett J. Tipple
brett.tipple@utah.edu

[1] Department of Biology, University of Utah, 257 South 1400 East, Salt Lake City, UT 84112, USA

[2] Global Change and Sustainability Center, University of Utah, 115 South 1460 East, Salt Lake City, UT 84112, USA

($\delta^{13}C$) isotope records of ancient plant ecology and hydrology from *n*-alkyl lipids (e.g., Berke et al. 2012; Diefendorf et al. 2015a; Douglas et al. 2015; Liddy et al. 2016; Tierney et al. 2013; Tipple et al. 2011; Uno et al. 2016). This has led to an intersection where ecologists, geologists, and climatologist share a common interest. As paleoclimatogists and geochemists have increased the applications of isotope analysis of leaf wax lipids to understand historical and ancient systems, plant ecologists, biochemists, and botanists have sought to better understand the biochemical and environmental controls on the $\delta^{2}H$ or $\delta^{13}C$ values of leaf waxes and other plant compounds (e.g., Gamarra and Kahmen 2015; Kahmen et al. 2013a, b; Ladd and Sachs 2017; Newberry et al. 2015; Oakes and Hren 2016; Sachse et al. 2010, 2015; Tipple et al. 2016; Zhang et al. 2017). The shared interest in these compounds has led to numerous synergistic collaborations between the biological, ecological, and geological communities (Diefendorf et al. 2015b; Lee et al. 2016; Sachse et al. 2012).

The $\delta^{2}H$ plant leaf wax compounds, particularly the *n*-alkyl lipids, are powerful tools to understand and reconstruct a plant's water environment (Dawson et al. 2002). The relationship between the $\delta^{2}H$ of plant source water and *n*-alkyl lipids is well established, as source water is the ultimate source of hydrogen to all plant compounds (Sachse et al. 2012). The $\delta^{2}H$ of *n*-alkyl lipids is also shaped by atmospheric exchange and leaf water ^{2}H-enrichment from evaporation from the leaf (Kahmen et al. 2013b; Tipple et al. 2015) as well as the biosynthetic fractionations that occur during the formation of the lipids (Schmidt et al. 2003), all of which add to the information encoded in the $\delta^{2}H$ values of *n*-alkyl lipids. The *n*-alkyl lipids (e.g., *n*-alkanes, fatty acids) are synthesized through the acetogenic pathway (Zhou et al. 2010). 3-phosphoglyceric acid, the precursor molecule for the acetogenic pathway and the intermediate, pyruvate, originating from the Calvin Cycle or a secondary metabolism. The acetogenic pathway results in a four-carbon butyryl chain with seven hydrogen atoms that through fatty acid synthesis is elongated to form a C_{16} or C_{18} fatty acid with the addition of two-carbon acetyl-CoA units (Zhou et al. 2010). On the initial butyryl chain, three hydrogen atoms originate from biosynthetic water, two from NADPH from the light reaction, and two from precursor acetyl-CoA from the chloroplast pyruvate (Cormier et al. 2018; Sachse et al. 2012; Schmidt et al. 2003; Zhou et al. 2010). Of the hydrogen atoms added during elongation within the chloroplast, 50% was derived from NADPH, 25% from the surrounding biosynthetic water, and the remaining 25% from chloroplast pyruvate (Cormier et al. 2018). These fatty acids are exported and further elongated in the endoplasmic reticulum, creating longer alkanoic acids and alkanes with hydrogen atoms derived from NADPH (50%), biosynthetic water (25%), and precursor pyruvate (25%) (Cormier et al. 2018). Several different metabolic pathways are used to produce NADPH and, thus, the relative importance of these pathways in the production of *n*-alkyl lipids will affect the $\delta^{2}H$ value (Cormier et al. 2018). Nonetheless, the primary source of NADPH in higher plants is photosynthesis, as demonstrated by the strong linear relationship between the $\delta^{2}H$ of source water and *n*-alkyl lipids (Sachse et al. 2012).

The $\delta^{13}C$ of *n*-alkyl lipids is useful to understand modern and past plant physiology and ecophysiology (Diefendorf and Freimuth 2017). The $\delta^{13}C$ values of plant material reflect photoassimilated CO_2 and fractionations associated with carbon fixation. During photosynthesis, CO_2 is fixed and converted to sugars and the $\delta^{13}C$ values of photosynthate are most strongly affected by the discrimination of ^{13}C by Rubisco—the enzyme that fixes CO_2. The $\delta^{13}C$ of photosynthate and its products is also a function of CO_2 diffusion, leaf conductance, and the concentrations of intercellular and atmospheric CO_2 (Farquhar et al. 1989). Also, photosynthetic pathway has a large control on the final $\delta^{13}C$ of products. The C_3 photosynthetic pathway is the most common and has the largest net fractionation between CO_2 and the plant material. The C_4 and Crassulacean acid metabolism (CAM) photosynthetic pathways spatially or temporally separate CO_2 fixation from carbon assimilation, respectively. As a result, the $\delta^{13}C$ of C_4 and CAM plant materials are less negative than those of C_3 plants. As with other plant tissues, the $\delta^{13}C$ of lipids reflects and records the photosynthetic pathway of the plant. In higher plants, the initial steps of *n*-alkyl lipid biosynthesis occur in the chloroplast, with carbon atoms originating from chloroplast pyruvate (Zhou et al. 2010). The elongation phase occurs in the endoplasmic reticulum, with the carbon atoms added during this phase originating from precursor pyruvate (Zhou et al. 2010). Thus, the carbon atoms in *n*-alkyl lipids can originate from both assimilatory carbohydrates as well as transported carbohydrates from storage organs (Schmidt et al. 2003). Nonetheless, there are fractionations during lipid biosynthesis related to the numerous biochemical branch points which control the relationship between the $\delta^{13}C$ of lipids, intermediates, and precursor molecules (Hayes 2001; Monson and Hayes 1980).

Coupling multiple isotope systems within a single plant tissue or compound can greatly expand the utility of isotope analysis (e.g., Mallette et al. 2017; Voelker et al. 2016). In this respect, linking the $\delta^{13}C$ and $\delta^{15}N$ values of plant tissues has increased the knowledge of carbon and nitrogen dynamics (e.g., Choi et al. 2005; Hobbie et al. 2017; Nasholm et al. 1998), while coupling $\delta^{13}C$ and $\delta^{18}O$ values from tree-ring cellulose has allowed for greater fidelity in the interpretation of climate archives from tree-ring record (e.g., Leavitt 2010; Szejner et al. 2016). Recently, the combination of $\delta^{13}C$, $\delta^{18}O$, and $\delta^{2}H$ values of leaf cellulose was used to trace the transition from juvenile to mature period in leaf expansion and to demonstrate that hydrogen and oxygen in cellulose are controlled by different biochemistry (Kimak et al. 2015).

The carbon and hydrogen isotope ratios of *n*-alkyl leaf wax lipids can be measured on the same individual compound with little to no additional purification or preparation. As *n*-alkyl leaf wax lipids are refractory in many geologic settings and can be isolated from soils, sediments, and rocks with straightforward procedures, the utility of these compounds is further amplified, as deeper time applications are possible. Strong relationships between a plant's carbon metabolism, plant functional type, and the δ^2H of *n*-alkyl lipids have been recognized (Chikaraishi and Naraoka 2007; Chikaraishi et al. 2004a; Cormier et al. 2018; Gamarra et al. 2016; Pedentchouk et al. 2008; Zhou et al. 2016), yet the majority of ancient and modern controlled studies on leaf wax lipids focus on either δ^2H or δ^{13}C values of these compounds exclusively. These concepts are just beginning to be applied to reconstruct paleoenvironments from leaf wax lipids isotope ratios (Magill et al. 2013; Tipple 2013; Tipple and Pagani 2010).

The mechanistic relationship between δ^2H and δ^{13}C values in *n*-alkyl lipids and how these values change during foliar development remains nascent. In broad-leaf species, variations in the δ^2H of *n*-alkanes have been shown to relate to periods of leaf development (Freimuth et al. 2017; Kahmen et al. 2011; Oakes and Hren 2016; Sachse et al. 2015; Tipple et al. 2013). Pedentchouk et al. (2008) measured both δ^2H and δ^{13}C values of *n*-alkanes from broad-leafed species throughout a season and showed variations in both δ^2H and δ^{13}C of *n*-alkanes during the study period; however, these isotopic changes were not monitored in relation to foliar development. Recently, several studies have compared the δ^2H of *n*-alkanes to δ^{13}C of bulk foliar material through the growing season and found that both the *n*-alkanes and structural carbon were synthesized from stored and recent assimilate in the initial and later growth periods, respectively (Freimuth et al. 2017; Newberry et al. 2015). However, the relationships between δ^2H and δ^{13}C of *n*-alkanes in context to leaf development have not yet been explored.

Here, we investigate the multiple carbon and water sources that can influence the isotopic composition of *n*-alkanes in leaves. We report the δ^2H and δ^{13}C values of *n*-alkanes, the δ^2H values of leaf, xylem, atmospheric, and stream waters, and the δ^{13}C values of bulk foliar material, along with *n*-alkane molecular distributions from three common riparian tree species: *Betula occidentalis*, *Populus angustifolia*, and *Acer negundo*. Materials from these species were collected in a natural montane ecosystem, at 15 intervals throughout the growing season. Materials were specifically collected from leaves that developed during the initial leaf flush. These species and ecosystem were selected, as the δ^2H value of stream water was known to remain relatively constant throughout the year and allowed for the effects of humidity and the δ^2H of atmospheric water vapor on the δ^2H of *n*-alkanes to be isolated. Concurrent collections of the δ^2H from *n*-alkanes, xylem, leaf, and stream water allowed us to monitor the relationship between xylem and leaf water on the biosynthetic fractionation of *n*-alkanes. Also, the paired collections of δ^{13}C values of *n*-alkanes and bulk leaf tissue provided information into the physiological and synthetic processes that connect these components of the leaf. Finally, the paired measurements of δ^2H and δ^{13}C of *n*-alkanes allowed us to evaluate how carbon metabolism and water environment are recorded within the same plant molecule, while jointly studying the effects of leaf ontogeny on these isotope systems. With this study, we sought to understand the temporal dynamics of coupled measurements of the δ^2H and δ^{13}C of *n*-alkanes and to determine the relationship between these isotope signatures and the heterotrophic and autotrophic processes that occur during foliar development and leaf expansion.

Materials and methods

Sample location and material collection

Materials from three individuals of *Betula occidentalis* Hook. (Western river birch), three individuals of *Populus angustifolia* James (narrowleaf cottonwood), and three individuals of *Acer negundo* L. (boxelder) were collected from a riparian environment near the Mill B South Fork of Big Cottonwood Creek in Big Cottonwood Canyon, Utah. Materials were collected from the same individuals on 15 dates throughout the 2010 Northern Hemisphere-growing season. Leaf samples were collected from the four cardinal directions from each individual and combined to reduce sun/shade variations. From each individual, approximately 4–8 buds or leaves were collected, combined, and stored in paper coin envelopes for leaf lipid and bulk carbon isotope analysis. The date on which the first full immature leaves were observed was described as "leaf flush" and occurred on DOY 141 for *B. occidentalis* and *A. negundo*, and DOY 146 for *P. angustifolia.* The date on which the first mature leaves were observed was noted as the mature phenophase and occurred on DOY 167 for *B. occidentalis* and *A. negundo*, and DOY 161 for *P. angustifolia.* The period including and between the "leaf flush" and the mature phenophase was termed the leaf expansion phenophase. The interval prior to "leaf flush" was described as the bud phenophase. Particular care was taken to only sample mature leaves from the initial leaf flush. These samples were dried for 48 h in a 50 °C oven immediately following collection.

Additional leaf samples were collected from the four cardinal directions of a single representative individual of the species above for water extraction. These samples were collected from the same representative of each of the three species throughout the season. Here, 4 leaves were collected and

amalgamated in 4-ml ashed glass vials for leaf water analysis. Stem samples were collected from the same individual that was sampled for leaf water analysis. Woody stems from the first branch point of the tree's trunk were collected and stored in 4-ml ashed glass vials. All leaf and stem water sample vials were capped, sealed with Parafilm®, and stored in a freezer until the time of processing.

Atmospheric water vapor was sampled using a cryo-trap following Helliker et al. (2002). Vapor samples were sampled on all collection days with the lone exception of the initial collection day. Briefly, atmospheric vapor was pumped through a glass cold trap submerged in a dry ice/ethanol slurry. After 1 h, the frozen atmospheric vapor was thawed and transferred to an ashed 4-ml vial, capped, and sealed with Parafilm®. The vial was stored in a freezer until the time of processing.

Water from Big Cottonwood Creek was sampled on each collection day. Water samples were collected in 4-ml ashed glass vials after rinsing the vial three times with water. Following collection, the vial was capped, sealed with Parafilm®, and stored in the freezer until the time of processing.

Plant water extraction and stable hydrogen isotope analysis of waters

Plant waters were extracted using a cryogenic vacuum water extraction method following West et al. (2006). After a complete extraction, the frozen plant water was thawed and transferred to an ashed 4-ml vial, capped, and sealed with Parafilm®. The vial was stored in a freezer until further processing. Prior to analysis, activated charcoal was added to plant waters to remove water-soluble organic compounds. After 48 h, the charcoal was removed and the water was transferred to ashed 2-ml autosampler vial. The 2-ml vial was stored in an 8 °C cooler until the time of analysis.

The stable hydrogen isotope ratios of plant waters, atmospheric water vapor, and stream water were analyzed on a Picarro model L1102-i water analyzer. Each water sample was analyzed four times (four consecutive replicate injections) with only the last two analyses being used. Unknowns were analyzed alongside a set of three in-house reference materials that were analyzed after every sixth unknown in an analytical sequence. The hydrogen isotope ratios of plant were normalized to the Vienna Standard Mean Ocean Water (VSMOW) scale using a two-point linear calibration of water primary reference materials, which had previously been standardized to the VSMOW scale [SIRFER *Zero* (0.1‰) and SIRFER *DI* (− 123.0‰)]. Precision for hydrogen isotope measurement of water was ± 2‰ (1σ, $n = 40$), as determined from secondary reference material [Evian, *EV* (− 72.5‰)].

All stable isotope ratios are reported in δ-notation:

$$\delta = \left[\left(\frac{R_{\text{sample}}}{R_{\text{std}}}\right) - 1\right] \quad (1)$$

where R represents the $^{2}H/^{1}H$ or $^{13}C/^{12}C$ abundance ratio, and R_{sample} and R_{std} are the ratios in the sample and standard, respectively. $\delta^{2}H$ values are expressed relative to the standard VSMOW, while $\delta^{13}C$ values are expressed relative to the standard Vienna Pee Dee Belemnite (VPDB).

Leaf preparation and stable carbon isotope analysis of bulk leaf material

Leaves were pulverized and homogenized in a solvent-washed ceramic mortar and pestle aided with liquid nitrogen. Ground leaf materials were transfer to an ashed 4-ml vial and stored until the time of processing. The stable carbon isotopes of bulk leaf material were analyzed using an EA 1110 CHN elemental analyzer (Carlo Erba, Milan, Italy) with a CONFLO III (Thermo Finnigan, Bremen, Germany) coupled to a Delta^{plus} isotope ratio mass spectrometer (Finnigan MAT, Bremen, Germany). Carbon isotope ratios of bulk plant material were normalized to the VPDB scale using a two-point linear calibration of primary reference materials, which had previously been standardized to the VPDB scale [UU-CN-1, glutamic acid (49.63‰) and UU-CN-2, glutamic acid (– 4.56‰)]. Primary reference materials were analyzed after every fifth unknown in an analytical sequence. Precision for carbon isotope measurement was ± 0.12‰ (1σ, $n = 32$), as determined from a secondary reference material [SIRFER Spinach (– 27.40‰)].

Lipid extraction, identification, and quantification

Lipids were extracted from 200 to 900 mg of ground leaf material with hexane by ultra-sonication (30 min × 2). The resulting extracts were concentrated under a gentle stream of purified nitrogen (N_2) gas using a FlexiVap Work Station (Glas-Col, Terre Haute, IN, USA) and were transferred to 4-ml glass vials. Extracts were then purified by column chromatography using 1 g deactivated silica gel (70–230 mesh) in an ashed Pasteur pipette, and eluted with 2 ml hexane to obtain the saturated hydrocarbons following Tipple and Pagani (2013).

Saturated hydrocarbons were analyzed using a TraceGC gas chromatograph (GC) with a TraceMS mass spectrometer (Thermo Finnigan, Milan, Italy). The GC was equipped with a split-splitless injector at 300 °C and a fused silica, DB-5 phase column (30 m × 0.25 mm I.D., 0.25 µm film thickness; J&W Scientific, Agilent Technologies, Santa Clara, CA, USA) with helium as the carrier at a flow of 1.5 ml/min. The GC oven temperature program was 60–320 °C at

15 °C/min with an isothermal for 30 min. High molecular *n*-alkanes were identified through comparison of elution times with known *n*-alkane standards.

Chain length distributions and concentrations of n-alkanes

Peak areas of high molecular weight *n*-alkanes were measured to quantify concentration and distribution. Concentrations were quantified using a 4-point calibration curve generated from reference materials of known concentration. The carbon preference index (CPI) was calculated following Marzi et al. (1993):

$$\mathrm{CPI} = \frac{(A_{23}+A_{25}+A_{27}+A_{29}+A_{31}+A_{33})+(A_{25}+A_{27}+A_{29}+A_{31}+A_{33}+A_{35})}{2(A_{24}+A_{26}+A_{28}+A_{30}+A_{32}+A_{34})} \quad (2)$$

where "*A*" represents the area of the individual *n*-alkane peaks. The average chain length (ACL) of *n*-alkanes was calculated:

$$\mathrm{ACL} = \frac{(A_{23}(23))+(A_{25}(25))+(A_{31}(27))+(A_{29}(29))+(A_{31}(31))+(A_{33}(33))+(A_{35}(35))}{(A_{23}+A_{25}+A_{27}+A_{29}+A_{31}+A_{33}+A_{35})} \quad (3)$$

Compound-specific hydrogen and carbon isotope analysis

Compound-specific hydrogen isotope analyses were performed at the SIRFER Laboratory, University of Utah using a Trace GC Ultra gas chromatograph (Thermo Electron Corporation, Milan, Italy) equipped with a split-splitless injector at 300 °C and a fused silica, DB-5 phase column (30 m × 0.25 mm I.D., 0.25 µm film thickness; J&W Scientific, Agilent Technologies, Santa Clara, CA, USA). Helium was the carrier, with a flow rate of 1.2 ml/min. The GC oven temperature program was 102–350 °C at 6 °C/min with an isothermal for 8 min. Following GC separation, *n*-alkanes were pyrolyzed at 1400 °C in a High Temperature Conversion system (Thermo Scientific, Bremen, Germany) and subsequently analyzed for hydrogen isotope ratios using a Delta V Plus isotope ratio mass spectrometer (Thermo Scientific, Bremen, Germany). The H_3^+ factor was determined daily prior to standard calibration and sample analysis. The average H_3^+ factor during these analyses was 2.42 ± 0.25 (1σ, n = 43). Individual *n*-alkane hydrogen isotope ratios were normalized to the VSMOW scale using a two-point linear calibration of *n*-alkane primary reference materials, which had previously been standardized to the VSMOW scale [*n*-C_{24} (– 36‰) and *n*-C_{28} (– 250‰)]. Primary reference materials were analyzed after every fifth unknown in an analytical sequence. Precision for *n*-alkanes hydrogen isotope determinations was ± 3‰ (1σ, n = 165), as determined from a secondary *n*-alkane reference material [*n*-C_{36} (– 240‰)]. The apparent fractionation between *n*-alkane and leaf water (ε_H) is defined as:

$$\varepsilon_H = \left[\left(\frac{R_{n-\mathrm{alkane}}}{R_{LW}}\right) - 1\right] \quad (4)$$

where R represents the $^2H/^1H$ abundance ratio, and $R_{n\text{-alkane}}$ and R_{LW} are the ratios in the *n*-alkane and leaf water, respectively.

Compound-specific carbon isotope analyses were also performed in the SIRFER Laboratory at the University of Utah. A 6890A GC (Hewlett-Packard Company, Palo Alto, CA, USA) employing a split–splitless injector held at a constant 310 °C with a fused silica, DB-5 phase column (30 m × 0.25 mm I.D., 0.25 µm film thickness; J&W Scientific, Agilent Technologies, Santa Clara, CA, USA) was used. Helium was the carrier, with a flow rate of 1.2 ml/min. The GC oven temperature program was 80–320 °C at 6 °C/min with an isothermal for 12 min. Compounds were subsequently combusted over nickel oxide, copper oxide, and platinum at 1000 °C using a GC Combustion III system (Thermo Quest Finnigan, Bremen, Germany) and analyzed for carbon isotope ratios using a Delta^{plus}XL isotope ratio mass spectrometer (Thermo Quest Finnigan, Bremen, Germany). Individual *n*-alkane carbon isotope ratios were normalized to the VPDB scale using a two-point linear calibration of *n*-alkane primary reference materials, which had previously been standardized to the VPDB scale [*n*-C_{18} (– 33.3‰) and *n*-C_{28} (– 29.0‰)]. Primary reference materials were analyzed after every fifth unknown in an analytical sequence. Arndt Schimmelmann's "*Mix A4*" [*n*-C_{16} (– 30.7‰), *n*-C_{17} (– 31.2‰), *n*-C_{18} (– 31.1‰), *n*-C_{19} (–33.2‰), *n*-C_{20} (– 32.4‰), *n*-C_{21} (– 29.1‰), *n*-C_{22} (– 32.9‰), *n*-C_{23} (– 31.8‰), *n*-C_{24} (– 33.3‰), *n*-C_{25} (–28.5‰), *n*-C_{26} (– 33.0‰), *n*-C_{27} (– 29.6‰), *n*-C_{28} (–32.2‰), *n*-C_{29} (– 30.1‰), and *n*-C_{30} (– 29.9‰)] was analyzed twice in each analytical sequence (n = 32) and had a measured accuracy of 0.1‰. Precision for *n*-alkanes carbon isotope determinations was ± 0.3‰ (1σ, n = 157), as determined from a co-injected secondary reference material [5α-androstane (– 30.1‰)]. The apparent fractionation between *n*-alkane and bulk leaf (ε_C) is defined as:

$$\varepsilon_C = \left[\left(\frac{R_{n-\mathrm{alkane}}}{R_{bulk}}\right) - 1\right] \quad (5)$$

where R represents the $^{13}C/^{12}C$ abundance ratio, and $R_{n\text{-alkane}}$ and R_{bulk} are the ratios in the n-alkane and bulk leaf, respectively.

Statistical analysis

Statistical analysis was completed using JMP Pro 13® (SAS Institute Inc., Cary, NC, USA). The isotope data from a given sampling day, species, and leaf developmental stage were compared using Student t tests to identify differences ($\alpha < 0.05$).

Results

Abundance and distribution of *n*-alkanes

The concentrations of individual n-alkane homologs and total n-alkanes relative to dry weight were determined (Table 1). Concentration data for each individual and all measured n-alkane homologs are reported in Table S1. In addition, the average chain length (ACL) values were calculated (Table 1). Here, we found that each species produced a unique distribution of n-alkanes with variations in distribution and concentration between the species and leaf developmental stage. *Betula occidentalis* produced n-C_{23} to n-C_{33} with n-C_{27}, n-C_{29}, and n-C_{31} being the most abundant homologs. The three *B. occidentalis* individuals had average concentrations of 243 ± 130, 89 ± 35, and 117 ± 44 μg g^{-1} over the sampling period for n-C_{27}, n-C_{29}, and n-C_{31}, respectively (Table 1). The total concentration of n-alkanes on all *B. occidentalis* individuals ranged from 44 to 1899 μg g^{-1} over the sampling period with an average of 486 ± 510 μg g^{-1}. In general, the total n-alkane concentration in *B. occidentalis* decreased 10-fold from the bud phenophase through leaf expansion (DOY 112 to 167) and then increased slightly during leaf maturation (DOY 179 to 239) and then decreased subsequently (Fig. 1). However, the relative distribution of n-alkanes varied throughout the leaf developmental stages with the n-C_{29}/n-C_{31} ratio varying from 2.04 to 8.94 in the bud to leaf flush (DOY 112 to 141) and then dropping precipitously to an average of 0.36 in the mature leaf (Table S1).

Populus angustifolia produced n-C_{23} to n-C_{31} with n-C_{27} and n-C_{29} being the most abundant homologs. In the three *P. angustifolia* individuals sampled, n-C_{29} (521 ± 153 μg g^{-1}) was the most abundant homolog on average, approximately two times more abundant than the next most abundant homolog, n-C_{27} (239 ± 76 μg g^{-1}) (Table 1). The average total concentration of n-alkanes on *P. angustifolia* individuals was 825 ± 342 μg g^{-1}. The total n-alkane concentrations in *P. angustifolia* were distinct from the other species and increased over from 43 to 1492 μg g^{-1} during leaf expansion (DOY 147 to 161) and then decreased during the mature phenophase (Fig. 1). However, the relative distribution of n-alkanes varied in *P. angustifolia* throughout the leaf developmental stages with the n-C_{27}/n-C_{29} ratio varying from an average value of 2.83 in the bud phenophase to leaf flush (DOY 112 to 146) to an average 0.14 in the mature leaf (Table S1).

The composition of n-alkanes on *Acer negundo* was n-C_{23} to n-C_{33}, with n-C_{31} as the most abundant and with n-C_{27} and n-C_{29} being roughly five-times less concentrated than n-C_{31}. The three *A. negundo* individuals sampled had an average n-C_{31} concentration of 550 ± 224 μg g^{-1}. *A. negundo* had an average total concentration of n-alkanes 1064 ± 224 μg g^{-1} with a range of 467 to 3876 μg g^{-1}. The total n-alkane concentration in *A. negundo* decreased significantly during the bud to leaf flush (DOY 112 to 141) and then remained relatively stable throughout the leaf expansion and mature leaf phenophases (Fig. 1). While the total n-alkane concentration remained stable, the relative distribution subtly varied across the season. The C_{27}/n-C_{29} ratio generally decreased from the initial leaf expansion phenophase to the mature leaf phenophase, while the n-C_{29}/n-C_{31} remained relatively stable during this period (Table 1).

We found that all species showed systematic changes in the average chain length (ACL) during the season and leaf developmental phenophases. Here, all species had ACL values that remained stable or decreased from bud to leaf flush (Fig. 1). The ACL of all species increased during the leaf expansion phenophase. ACL stabilized once the leaves of *P. angustifolia* and *A. negundo* matured, while the ACL of *B. occidentalis* continued to increase until DOY 239, after which it stabilized. *B. occidentalis* individuals had an average ACL of 27.9 ± 1.3 with a range from 26.3 to 29.8. *P. angustifolia* individuals had an average ACL of 28.2 ± 0.7 with a range from 27.3 to 28.9. Finally, *A. negundo* individuals had an average ACL of 30.3 ± 0.4 with a range from 29.5 to 30.7.

Hydrogen isotopes of plant and environmental waters

The hydrogen isotope values of stream water and atmospheric water vapor are presented in Table 2. The mean hydrogen isotope value of stream water (δ^2H_{MW}) was -130 ± 1‰ (1σ, $n = 15$; Table 2). The δ^2H_{MW} of Big Cottonwood Creek waters did not vary significantly during the studied interval as the major source of water derived from upper elevation snow melt (Roden and Ehleringer 2000). The mean hydrogen isotope value of atmospheric water vapor (δ^2H_V) was -172 ± 24‰ (1σ, $n = 14$) and ranged from -233 to -132‰. The δ^2H_V varied over 100‰ due to changes in moisture source regions. Vapor was most

Table 1 Average concentrations of individual and total *n*-alkanes and molecular distrtibutions of *n*-alkanes from three riparian tree species

Ordinal date	Phenophase	[n-C_{27}] (mg g^{-1})		SD	[n-C_{29}] (mg g^{-1})		SD	[n-alkane] (mg g^{-1})		SD	CPI		SD	ACL		SD
Betula occidentalis																
112	Bud	0.8807	±	0.7449	0.2780	±	0.1742	1.341	±	1.067	35.6	±	9.7	27.68	±	0.46
123	Bud	1.2350	±	0.5486	0.3511	±	0.0287	1.899	±	0.621	41.9	±	11.3	27.64	±	0.41
132	Bud	0.4186	±	0.1430	0.1076	±	0.0140	0.663	±	0.230	27.0	±	1.7	27.23	±	0.48
137	Bud	0.2141	±	0.1351	0.0415	±	0.0211	0.327	±	0.225	46.7	±	19.7	26.87	±	0.48
141	Leaf expansion	0.1223	±	0.0378	0.0210	±	0.0013	0.181	±	0.055	29.6	±	0.5	26.74	±	0.39
146	Leaf expansion	0.0849	±	0.0342	0.0102	±	0.0026	0.139	±	0.062	35.0	±	4.8	26.28	±	0.46
153	Leaf expansion	0.0995	±	0.0507	0.0127	±	0.0048	0.166	±	0.091	23.8	±	5.9	26.35	±	0.51
161	Leaf expansion	0.0843	±	0.0249	0.0748	±	0.0932	0.213	±	0.120	45.4	±	27.0	27.07	±	1.24
167	Leaf expansion	0.0192	±	0.0160	0.0063	±	0.0057	0.044	±	0.031	20.4	±	3.2	26.90	±	1.49
179	Mature	0.0526	±	0.0324	0.0246	±	0.0028	0.162	±	0.079	17.7	±	2.3	28.35	±	0.98
195	Mature	0.0683	±	0.0275	0.0538	±	0.0180	0.285	±	0.035	26.7	±	1.5	29.01	±	0.98
216	Mature	0.1334	±	0.0592	0.1412	±	0.0829	0.703	±	0.246	22.5	±	2.0	29.54	±	0.71
239	Mature	0.1105	±	0.0402	0.1092	±	0.0264	0.577	±	0.072	18.9	±	0.8	29.73	±	0.40
250	Mature	0.0555	±	0.0146	0.0509	±	0.0248	0.276	±	0.069	18.7	±	0.7	29.75	±	0.22
274	Mature	0.0622	±	0.0246	0.0570	±	0.0189	0.313	±	0.118	18.0	±	3.4	29.73	±	0.29
Populus angustifolia																
112	Bud	0.3485	±	0.0630	0.1069	±	0.0085	0.515	±	0.062	24.5	±	9.5	27.36	±	0.15
123	Bud	0.4687	±	0.3604	0.1339	±	0.1160	0.718	±	0.621	29.0	±	11.0	27.30	±	0.13
132	Bud	0.4851	±	0.0283	0.1586	±	0.0068	0.741	±	0.034	23.1	±	8.4	27.37	±	0.12
137	Bud	0.2815	±	0.0628	0.1003	±	0.0276	0.431	±	0.115	26.9	±	14.6	27.39	±	0.09
141	Bud	0.3292	±	0.1118	0.1392	±	0.0395	0.519	±	0.164	25.8	±	7.1	27.50	±	0.01
146	Leaf expansion	0.3156	±	0.1007	0.3379	±	0.3288	0.699	±	0.446	32.1	±	9.8	27.81	±	0.44
153	Leaf expansion	0.3971	±	0.1127	0.9449	±	0.3303	1.447	±	0.454	21.5	±	1.8	28.42	±	0.15
161	Leaf expansion	0.1758	±	0.1116	1.2525	±	0.4393	1.492	±	0.590	34.5	±	8.1	28.81	±	0.09
167	Mature	0.0985	±	0.0227	1.1023	±	0.3261	1.251	±	0.277	46.8	±	48.8	28.86	±	0.06
179	Mature	0.0955	±	0.0316	0.5549	±	0.1473	0.705	±	0.184	23.4	±	12.2	28.78	±	0.04
195	Mature	0.1110	±	0.0024	0.6711	±	0.1524	0.840	±	0.145	31.7	±	7.1	28.76	±	0.04
216	Mature	0.1228	±	0.0243	0.7676	±	0.0360	0.965	±	0.054	25.6	±	3.4	28.95	±	0.32
239	Mature	–	±	–	–	±	–	–	±	–	–	±	–	–	±	–
250	Mature	0.0513	±	0.0241	0.4917	±	0.1416	0.579	±	0.187	30.9	±	21.9	28.82	±	0.06
274	Mature	0.0669	±	0.0059	0.5335	±	0.0399	0.644	±	0.032	23.9	±	6.7	28.77	±	0.05
Acer negundo																
112	Bud	0.2798	±	0.1458	1.9187	±	0.2296	3.876	±	0.376	4.8	±	0.6	30.67	±	0.41
123	Bud	0.1562	±	0.1436	0.2700	±	0.3185	0.873	±	0.302	3.7	±	3.6	29.62	±	0.60
132	Bud	0.0810	±	0.0558	0.3696	±	0.2916	0.878	±	0.436	5.4	±	4.7	29.54	±	0.51

Table 1 (continued)

Ordinal date	Phenophase	[n-C_{27}] (mg g^{-1})		SD	[n-C_{29}] (mg g^{-1})		SD	[n-alkane] (mg g^{-1})		SD	CPI		SD	ACL		SD
137	Bud	–	±	–	–	±	–	–	±	–	–	±	–	–	±	–
141	Leaf expansion	0.0957	±	0.0234	0.3959	±	0.0840	0.824	±	0.276	7.0	±	2.1	29.85	±	0.59
146	Leaf expansion	0.0867	±	0.0074	0.3799	±	0.0769	0.733	±	0.156	5.7	±	0.8	30.00	±	0.21
153	Leaf expansion	0.0683	±	0.0118	0.2683	±	0.0794	0.559	±	0.154	5.5	±	1.7	29.91	±	0.21
161	Leaf expansion	0.1632	±	0.0462	0.5590	±	0.0916	1.177	±	0.249	5.1	±	1.1	30.23	±	0.08
167	Leaf expansion	0.1674	±	0.0358	0.5656	±	0.1444	1.177	±	0.243	5.9	±	1.4	30.24	±	0.05
179	Mature	0.0743	±	0.0347	0.3806	±	0.1476	0.645	±	0.268	9.7	±	0.9	30.62	±	0.02
195	Mature	0.1335	±	0.1229	0.6722	±	0.5655	1.116	±	0.962	12.0	±	2.6	30.60	±	0.08
216	Mature	0.0719	±	0.0121	0.3951	±	0.0986	0.620	±	0.124	10.8	±	1.6	30.61	±	0.11
239	Mature	0.1968	±	0.1974	0.8849	±	0.7935	1.440	±	1.399	11.9	±	1.7	30.50	±	0.18
250	Mature	0.0492	±	0.0087	0.3534	±	0.1428	0.516	±	0.189	13.2	±	2.2	30.71	±	0.17
274	Mature	0.0574	±	0.0117	0.2891	±	0.0738	0.467	±	0.076	10.0	±	2.9	30.50	±	0.32

^{2}H-depleted early in the growing season, reflecting cooler air masses originating from the Northern Pacific.

The hydrogen isotope values of stem and leaf waters are provided in Table 2 and shown in Fig. 2. Here, we found that hydrogen isotope values of stem waters (δ^2H_{XW}) in all species were more ^{2}H-enriched values in the initial growing season and became relatively more ^{2}H-depleted prior to leaf maturity. The δ^2H_{XW} from all species ranged from − 87 to − 145‰ (Table 2). Mean δ^2H_{XW} of *B. occidentalis*, *P. angustifolia*, and *A. negundo* was − 125 ± 13, − 129 ± 9, and − 116 ± 15‰ (1σ, $n = 15$ for each species), respectively. Mean δ^2H_{XW} of *B. occidentalis* and *P. angustifolia* was not different, while δ^2H_{XW} from *A. negundo* was significantly different from the other two species (*t* test, $p = 0.0191$ and 0.0017, respectively). Following the bud and leaf expansion phenophases, the δ^2H_{XW} for all species stabilized and remained relatively constant for the remainder of the growing season (Fig. 2). Mean δ^2H_{XW} of *B. occidentalis*, *P. angustifolia*, and *A. negundo* during the mature leaf phenophase was − 138 ± 3‰ (1σ, $n = 6$), − 135 ± 5‰ (1σ, $n = 7$), and − 125 ± 6‰ (1σ, $n = 6$), respectively. Additionally, the δ^2H_{XW} of *B. occidentalis* and *P. angustifolia* of each phenophase was not significantly different, while the δ^2H_{XW} of *A. negundo* was significantly different from *P. angustifolia* during the bud phenophase (*t* test, $p = 0.0182$) and both *B. occidentalis* and *P. angustifolia* during the mature leaf phenophase (*t*-test, $p = 0.0002$ and 0.0010, respectively). In addition, the pooled mean δ^2H_{XW} of all species during the mature phenophase was not significantly different than δ^2H_{MW}; however, the mean δ^2H_{XW} of each individual species during the mature phenophase was significantly different than δ^2H_{MW} (*t* test, all $p < 0.006$).

The hydrogen isotope values of leaf waters (δ^2H_{LW}) varied considerably during the growing season, ranging from − 38 to − 157‰. Mean δ^2H_{LW} of *B. occidentalis*, *P. angustifolia*, and *A. negundo* was − 92 ± 20‰ (1σ, $n = 15$), − 89 ± 19‰ (1σ, $n = 14$), and − 83 ± 33‰ (1σ, $n = 15$), respectively. The overall mean δ^2H_{LW} was not different among species, nor was the mean δ^2H_{LW} for each leaf developmental phenophase. Generally, δ^2H_{LW} and δ^2H_{XW} were relatively similar during the bud and leaf expansion phenophases, with δ^2H_{LW} being slightly less negative, while as the season progressed, δ^2H_{LW} became increasingly less negative compared to δ^2H_{XW} (Fig. 2). The difference (Δ) between δ^2H_{LW} and δ^2H_{XW} was 9 ± 21‰ (1σ, $n = 10$), 20 ± 13‰ (1σ, $n = 12$), and 56 ± 23‰ (1σ, $n = 22$) for the bud, leaf expansion, and mature phenophases, respectively. The δ^2H_{LW} was positively correlated with δ^2H_V ($R^2 = 0.72$, $p < 0.0001$) from leaf maturity until DOY 239.

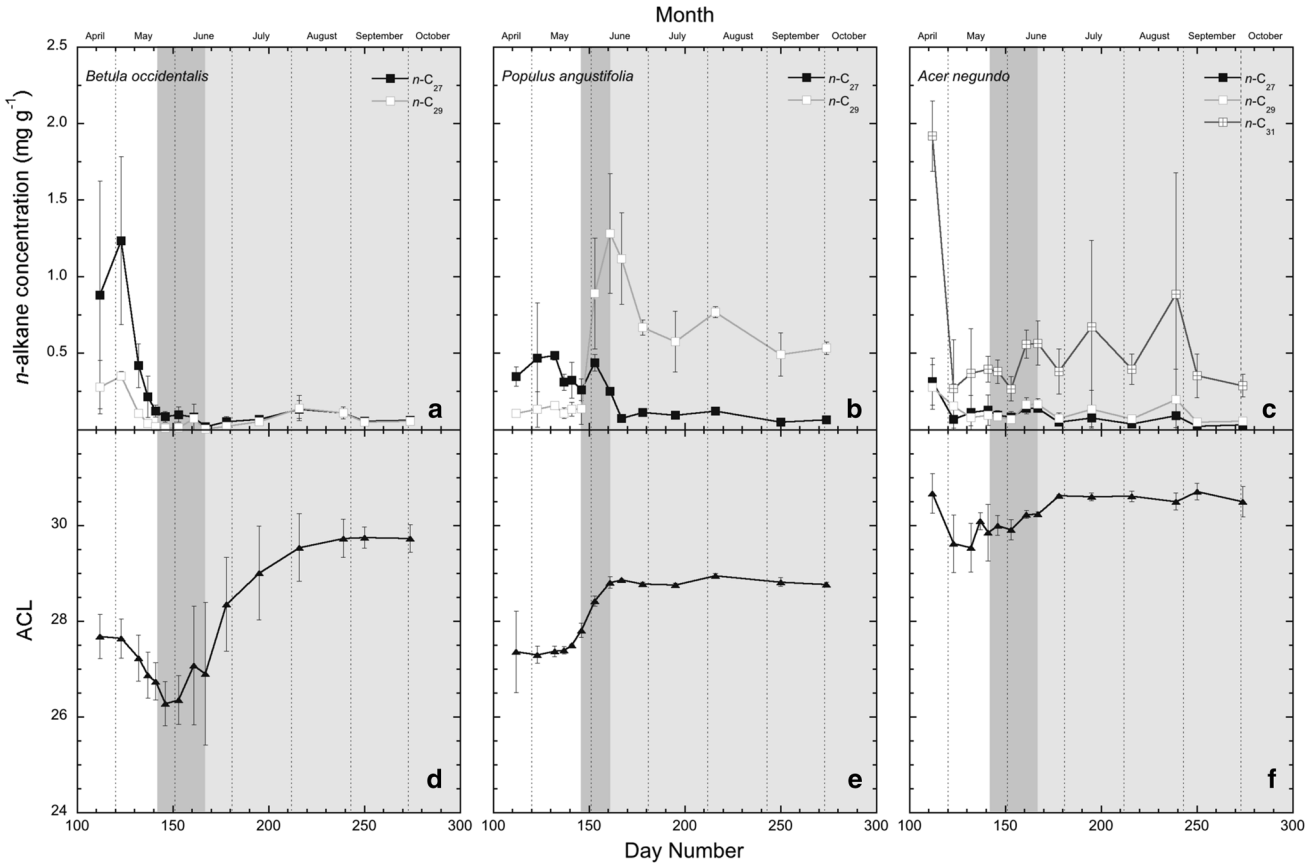

Fig. 1 Concentration of *n*-C_{27}, *n*-C_{29}, and *n*-C_{31} alkanes on buds and leaves of **a** *Betula occidentalis*, **b** *Populus angustifolia*, and **c** *Acer negundo*. Concentration data from *n*-C_{27}, *n*-C_{29}, and *n*-C_{31} are shown in closed, open, and crossed squares. Error bars represent the standard deviations around the mean of three individuals from each species. Average chain length of *n*-alkane from bud and leaf waxes, **d** *B. occidentalis*, **e** *P. angustifolia*, and **f** *A. negundo*. Error bars represent the standard deviations around the mean of the three individuals from each species used in this study. Colored areas correspond to the bud (white), leaf expansion (dark gray), and mature leaf (light gray) phenophases

Hydrogen isotopes of *n*-alkanes and fractionations between *n*-alkanes and leaf water

The hydrogen isotope values of prominent *n*-alkane homologs are reported in Table 3 and Fig. 2. Here, the δ^2H of *n*-C_{27} and *n*-C_{29} was measured in *B. occidentalis*, while it was only possible to measure *n*-C_{31} in *A. negundo*. While hydrogen isotope analysis was conducted on all homologs of sufficient abundance, we report and discuss the hydrogen isotope values of only the most abundant homolog for each species ($\delta^2H_{n\text{-alkane}}$). Nonetheless, the δ^2H of *n*-C_{27} and *n*-C_{29} from *B. occidentalis* was highly correlated ($R^2 = 0.93$, $p < 0.0001$). The δ^2H of *n*-C_{27} and *n*-C_{29} from *P. angustifolia* has been previously published (Tipple et al. 2013) and will not be extensively described here.

During specific phenophases, distinct patterns in the $\delta^2H_{n\text{-alkane}}$ of *B. occidentalis* and *A. negundo* were observed. In both species, the initial $\delta^2H_{n\text{-alkane}}$ values during the bud phenophase were the most negative and became less negative prior to leaf flush. A similar pattern was observed in *P. angustifolia*. During the transition from bud to leaf flush, the $\delta^2H_{n\text{-alkane}}$ of *B. occidentalis*, *P. angustifolia*, and *A. negundo* became more enriched by 20, 57, and 35‰, respectively. During leaf expansion, $\delta^2H_{n\text{-alkane}}$ of *B. occidentalis* continued to became more ^{2}H-enriched by 42‰, while the $\delta^2H_{n\text{-alkane}}$ of *A. negundo* stabilized, becoming only 2‰ more ^{2}H-enriched. In comparison, *P. angustifolia* became more ^{2}H-depleted by 11‰. From bud through leaf expansion, the total enrichment in ^{2}H for *B. occidentalis* (DOY 112 to 167), *P. angustifolia* (DOY 112 to 161), and *A. negundo* (DOY 112 to 167) was 63, 46, and 37‰, respectively. The enrichment pattern in $\delta^2H_{n\text{-alkane}}$ corresponding to the same interval in that δ^2H_{XW} became more ^{2}H-depleted. After the leaf expansion phenophase, the $\delta^2H_{n\text{-alkane}}$ values became very stable, where the mean $\delta^2H_{n\text{-alkane}}$ value remained at -195 ± 5‰ (1σ, $n = 6$), -219 ± 3‰ (1σ, $n = 7$), and -214 ± 2‰ (1σ, $n = 6$) for *B. occidentalis*, *P. angustifolia*, and *A. negundo*, respectively.

Table 2 Hydrogen isotope values of Big Cottonwood Creek water, atmospheric water vapors as well as xylem and leaf water from three riparian tree species

Ordinal date	δ^2H stream (‰, VSMOW)	δ^2H vapor (‰, VSMOW)	*Betula occidentalis*						*Populus angustifolia*						*Acer negundo*					
			Phenophase	δ^2H stem (‰, VSMOW)		SD	δ^2H leaf (‰, VSMOW)		SD	Phenophase	δ^2H stem (‰, VSMOW)		SD	δ^2H leaf (‰, VSMOW)		SD	Phenophase	δ^2H stem (‰, VSMOW)		SD	δ^2H leaf (‰, VSMOW)		SD
112	− 132.2	–	Bud	− 118.2	±	0.0	− 107.4	±	–	Bud	− 123.1	±	0.3	–	±	–	Bud	− 116.8	±	0.0	− 157.3	±	0.9
123	− 131.2	− 172.9	Bud	− 100.3	±	0.3	− 100.6	±	0.5	Bud	− 117.8	±	0.2	− 93.2	±	0.0	Bud	− 86.9	±	0.4	− 80.6	±	2.2
132	− 131.5	− 233.4	Bud	− 113.1	±	0.0	− 109.4	±	0.2	Bud	− 110.2	±	1.1	− 99.6	±	1.2	Bud	− 89.3	±	0.2	− 87.0	±	1.1
137	− 131.2	− 185.5	Bud	− 119.0	±	0.0	− 116.6	±	–	Bud	− 132.0	±	0.2	− 100.4	±	–	Bud	− 109.5	±	0.1	− 73.2	±	0.5
141	− 130.5	− 157.5	Leaf expansion	− 107.2	±	–	− 84.7	±	2.1	Bud	− 120.7	±	0.1	− 85.2	±	0.1	Leaf expansion	− 101.9	±	0.4	− 82.1	±	0.4
146	− 130.1	− 159.6	Leaf expansion	− 114.5	±	0.7	− 99.6	±	0.3	Leaf expansion	− 120.4	±	0.7	− 93.1	±	0.5	Leaf expansion	− 108.3	±	–	− 71.1	±	0.0
153	− 129.4	− 187.6	Leaf expansion	− 120.7	±	–	− 122.4	±	1.0	Leaf expansion	− 127.1	±	0.2	− 115.7	±	0.5	Leaf expansion	− 114.7	±	0.8	− 105.6	±	0.5
161	− 127.9	− 168.9	Leaf expansion	− 130.8	±	0.9	− 99.7	±	–	Leaf expansion	− 135.8	±	0.1	− 96.1	±	0.4	Leaf expansion	− 130.4	±	0.2	− 95.3	±	0.3
167	− 129.3	− 169.0	Leaf expansion	− 133.1	±	0.2	− 87.2	±	0.2	Mature	− 133.4	±	0.6	− 114.7	±	1.1	Leaf expansion	− 132.4	±	–	− 99.1	±	0.8
179	− 130.2	− 186.5	Mature	− 139.4	±	0.3	− 98.4	±	–	Mature	− 133.5	±	0.1	− 111.8	±	0.6	Mature	− 133.7	±	0.1	− 132.1	±	0.0
195	− 129.9	− 167.8	Mature	− 135.8	±	1.4	− 85.4	±	–	Mature	− 133.9	±	0.1	− 75.9	±	–	Mature	− 130.6	±	0.2	− 74.7	±	0.5
216	− 129.6	− 139.0	Mature	− 136.3	±	–	− 81.9	±	0.5	Mature	− 131.2	±	–	− 68.4	±	1.1	Mature	− 122.5	±	0.5	− 66.6	±	0.8
239	− 129.0	− 132.3	Mature	− 139.9	±	0.2	− 59.0	±	1.2	Mature	− 133.3	±	0.9	− 60.6	±	0.5	Mature	− 123.5	±	0.3	− 41.6	±	0.2
250	− 129.8	− 168.9	Mature	− 133.3	±	0.3	− 65.2	±	0.3	Mature	− 136.1	±	0.7	− 69.1	±	0.9	Mature	− 120.1	±	0.4	− 38.3	±	0.2
274	− 127.5	− 176.1	Mature	− 140.6	±	0.4	− 56.2	±	–	Mature	− 145.3	±	0.8	− 61.1	±	0.4	Mature	− 119.2	±	0.1	− 39.5	±	0.0

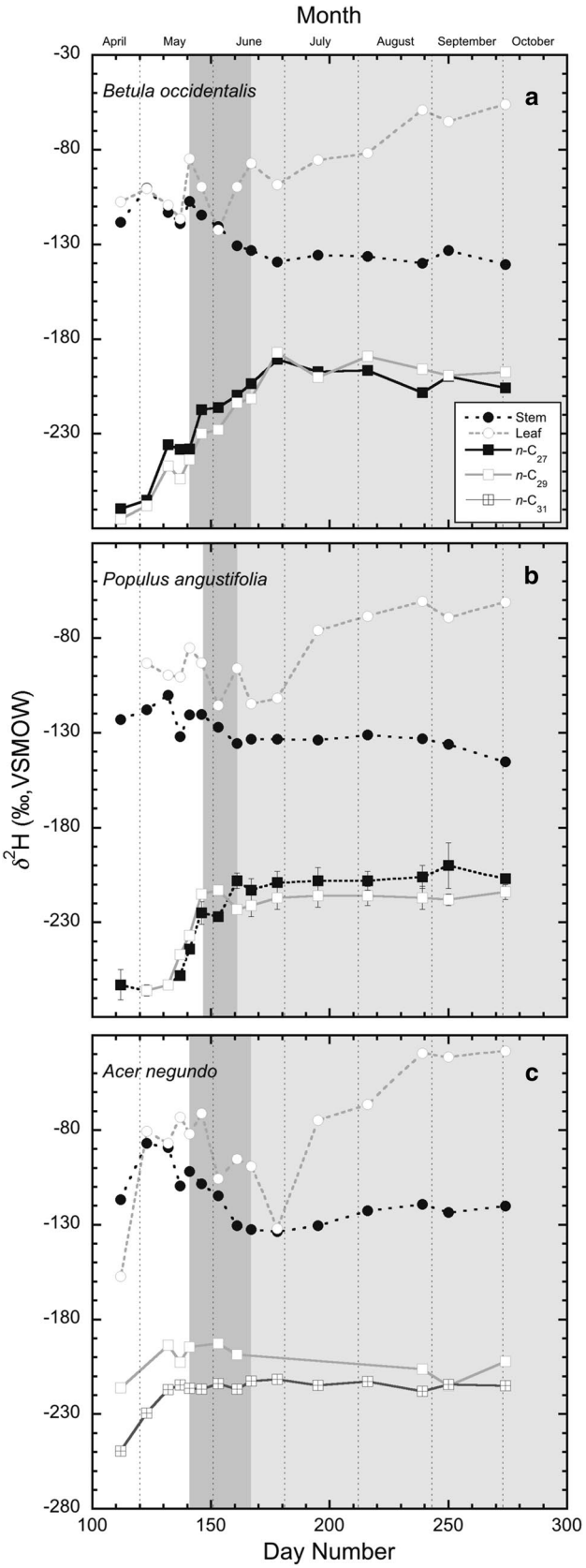

Fig. 2 Hydrogen isotope values of stem water, leaf water, and *n*-alkanes from **a** *Betula occidentalis*, **b** *Populus angustifolia*, and **c** *Acer negundo* during the studied interval. Hydrogen isotope values of stem and leaf water are shown in closed and open circles, while data from n-C_{27}, n-C_{29}, and n-C_{31} are shown in closed, open, and crossed squares, respectively. Error bars represent the standard deviations around the mean of three *P. angustifolia* specimens. Colored areas correspond to the bud (white), leaf expansion (dark gray), and mature leaf (light gray) phenophases

The apparent hydrogen isotope fractionation (ε_H) between $\delta^2H_{n\text{-alkane}}$ and δ^2H_{LW}, shown in Fig. 3, varied systematically across the growing season for all species. In general, we found that the initial ε_H values became relatively less negative from the bud phenophase through the leaf expansion phenophase. After leaf expansion, the ε_H values became more negative. The period from leaf flush to full leaf expansion is known to be the interval of wax synthesis in broadleafed angiosperms (Freimuth et al. 2017; Kahmen et al. 2011; Oakes and Hren 2016; Tipple et al. 2013). During this interval, we found that the pooled mean ε_H value for all species was -132 ± 18‰ (1σ, $n=13$) and the individual mean ε_H values were -131 ± 22‰ (1σ, $n=5$), -124 ± 17‰ (1σ, $n=3$), -137 ± 15‰ (1σ, $n=5$) for *B. occidentalis*, *P. angustifolia*, and *A. negundo*, respectively. Following the leaf expansion and wax synthesis, ε_H values for all species gradually became more negative due to the ^{2}H-enrichment in the leaf water (Fig. 3).

Carbon isotopes of *n*-alkanes and bulk leaf materials

The carbon isotope values of bulk leaf material ($\delta^{13}C_{bulk}$) for all species are reported in Table 4 and Fig. 4. Within all species, a defined ^{13}C-enrichment was observed in $\delta^{13}C_{bulk}$ values during the bud and leaf expansion phenophases. Here, all species showed a slight ^{13}C-depletion, followed by a ^{13}C-enrichment prior to leaf flush (Fig. 4). The least negative $\delta^{13}C_{bulk}$ values were observed at or immediately following leaf flush, with values of -28.0, -29.5, and -27.7‰ for *B. occidentalis*, *P. angustifolia*, and *A. negundo*, respectively. $\delta^{13}C_{bulk}$ subsequently became more negative during the leaf expansion phenophase by 2.1, 0.4, and 1.6‰ for *B. occidentalis*, *P. angustifolia*, and *A. negundo*, respectively. Following leaf expansion, the $\delta^{13}C_{bulk}$ in all species remained stable through the growing season, where the mean $\delta^{13}C_{bulk}$ was -29.7 ± 0.3‰ (1σ, $n=6$), -31.3 ± 0.3‰ (1σ, $n=7$), and -30.1 ± 0.2‰ (1σ, $n=6$) for *B. occidentalis*, *P. angustifolia*, and *A. negundo*, respectively.

The carbon isotope values of prominent *n*-alkane homologs are reported in Table 4 and Fig. 4. The $\delta^{13}C$ of n-C_{27} and n-C_{29} was measured in all samples from three individuals of both *B. occidentalis* and *P. angustifolia*, with n-C_{27} and n-C_{29} the most abundant homolog for either species, respectively. The $\delta^{13}C$ of n-C_{29} and n-C_{31}

Table 3 Hydrogen isotope values of *n*-alkanes from the three species

Ordinal Date	*Betula occidentalis*							*Populus angustifolia*							*Acer negundo*						
	Phenophase	δ^2H *n*-C_{27} (‰, VPDB)		SD	δ^2H *n*-C_{29} (‰, VPDB)		SD	Phenophase	δ^2H *n*-C_{27} (‰, VPDB)		SD	δ^2H *n*-C_{29} (‰, VPDB)		SD	Phenophase	δ^2H *n*-C_{29} (‰, VPDB)		SD	δ^2H *n*-C_{31} (‰, VPDB)		SD
112	Bud	− 269.5	±	n/a	− 274.9	±	n/a	Bud	− 269.0	±	6.5	− 267.5	±	10.6	Bud	− 216.2	±	n/a	− 249.6	±	n/a
123	Bud	− 265.0	±	n/a	− 267.9	±	n/a	Bud	− 267.7	±	1.3	− 269.3	±	2.9	Bud	–	±	n/a	− 229.5	±	16.2
132	Bud	− 235.8	±	n/a	− 247.1	±	n/a	Bud	− 262.8	±	5.4	− 260.9	±	2.6	Bud	− 193.6	±	n/a	− 217.1	±	7.1
137	Bud	− 238.3	±	n/a	− 253.7	±	n/a	Bud	− 257.9	±	0.3	− 246.2	±	1.4	Bud	− 202.6	±	n/a	− 214.6	±	7.4
141	Leaf expansion	− 238.0	±	n/a	− 243.7	±	n/a	Bud	− 238.5	±	7.1	− 226.9	±	10.0	Leaf expansion	− 194.5	±	n/a	− 216.4	±	5.5
146	Leaf expansion	− 217.3	±	n/a	− 229.9	±	n/a	Leaf expansion	− 223.7	±	2.5	− 210.8	±	5.2	Leaf expansion	–	±	n/a	− 216.8	±	3.2
153	Leaf expansion	− 216.2	±	n/a	− 227.8	±	n/a	Leaf expansion	− 213.5	±	4.7	− 207.8	±	2.2	Leaf expansion	− 192.6	±	n/a	− 213.8	±	0.7
161	Leaf expansion	− 209.6	±	n/a	− 213.6	±	n/a	Leaf expansion	− 217.8	±	11.1	− 221.5	±	3.8	Leaf expansion	− 198.6	±	n/a	− 216.8	±	6.1
167	Leaf expansion	− 203.6	±	n/a	− 211.5	±	n/a	Mature	− 217.1	±	3.5	− 224.9	±	3.3	Leaf expansion	–	±	n/a	− 212.6	±	4.3
179	Mature	− 190.7	±	n/a	− 187.0	±	n/a	Mature	− 209.5	±	1.8	− 215.3	±	2.6	Mature	–	±	n/a	− 211.7	±	3.9
195	Mature	− 197.3	±	n/a	− 200.0	±	n/a	Mature	− 213.9	±	5.2	− 218.8	±	2.1	Mature	–	±	n/a	− 214.9	±	4.1
216	Mature	− 196.5	±	n/a	− 189.2	±	n/a	Mature	− 209.4	±	4.5	− 217.6	±	3.6	Mature	–	±	n/a	− 212.7	±	5.3
239	Mature	− 208.2	±	n/a	− 195.9	±	n/a	Mature	− 211.8	±	8.1	− 222.8	±	5.4	Mature	− 206.2	±	n/a	− 217.9	±	n/a
250	Mature	− 199.6	±	n/a	− 199.3	±	n/a	Mature	− 209.3	±	9.9	− 219.4	±	1.8	Mature	− 214.9	±	n/a	− 214.5	±	1.1
274	Mature	− 205.8	±	n/a	− 197.5	±	n/a	Mature	− 215.1	±	8.0	− 217.2	±	4.0	Mature	− 202.3	±	n/a	− 215.0	±	6.7

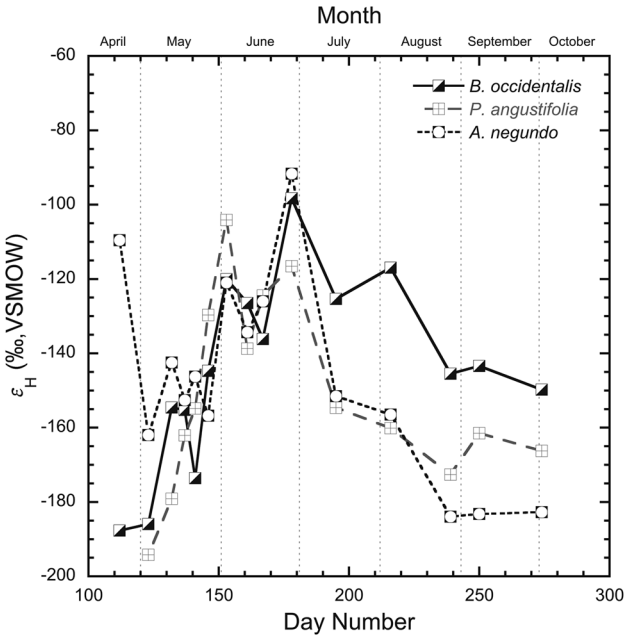

Fig. 3 Apparent fractionation between the hydrogen isotope values of leaf water and *normal* alkanes from *Betula occidentalis*, *Populus angustifolia*, and *Acer negundo* during the studied period

was measured in all samples from three individuals of *A. negundo*, with *n*-C_{31} being the most abundant homolog (Table S2). We found that the $\delta^{13}C$ of *n*-C_{27} and *n*-C_{29} from *B. occidentalis* and *P. angustifolia* was highly correlated ($R^2 = 0.74$, $p < 0.0001$; $R^2 = 0.60$, $p = 0.0006$, respectively), as was the $\delta^{13}C$ of *n*-C_{29} and *n*-C_{31} from *A. negundo* ($R^2 = 0.99$, $p < 0.0001$). Here, we discuss the carbon isotope values of only the most abundant homolog for each species ($\delta^{13}C_{n\text{-alkane}}$) and, thus, we focus our description and discussion on $\delta^{13}C$ of *n*-C_{27}, *n*-C_{29}, and *n*-C_{31} for *B. occidentalis*, *P. angustifolia*, and *A. negundo*, respectively.

As with $\delta^2H_{n\text{-alkane}}$, the $\delta^{13}C_{n\text{-alkane}}$ varied systematically during specific phenological intervals in each species. Where the patterns in $\delta^2H_{n\text{-alkane}}$ and $\delta^{13}C_{bulk}$ were generally similar between the species, the patterns in $\delta^{13}C_{n\text{-alkane}}$ were relatively unique for each species in this study. During the bud phenophase and prior to leaf flush, the $\delta^{13}C_{n\text{-alkane}}$ of both *B. occidentalis* and *P. angustifolia* became more ^{13}C-depleted (− 1.2 and − 1.7‰, respectively), whereas the $\delta^{13}C_{n\text{-alkane}}$ of *A. negundo* became more ^{13}C-enriched by 0.6‰. During leaf expansion, the $\delta^{13}C_{n\text{-alkane}}$ of both *B. occidentalis* and *A. negundo* continued to become ^{13}C-depleted by − 1.3 and − 4.2‰, respectively. During this interval, the $\delta^{13}C_{n\text{-alkane}}$ of *P. angustifolia* abruptly became more ^{13}C-enriched by 2.1‰. In the mature leaf phenophase, $\delta^{13}C_{n\text{-alkane}}$ values in all species were steady, where the mean $\delta^{13}C_{n\text{-alkane}}$ values were − 33.8 ± 0.3‰ (1σ, $n = 6$), − 34.3 ± 0.3‰ (1σ, $n = 7$), and − 37.3 ± 0.4‰ (1σ, $n = 6$) for *B. occidentalis*, *P. angustifolia*, and *A. negundo*, respectively.

The apparent carbon isotope fractionation (ε_C) between $\delta^{13}C_{n\text{-alkane}}$ and $\delta^{13}C_{bulk}$ is shown in Fig. 5. As with ε_H, ε_C varied systematically across the growing season for all species. In general, we found that the ε_C values became relatively more negative during the bud phenophase for *B. occidentalis* and *P. angustifolia*, while ε_C values became relatively less negative during the bud phenophase in *A. negundo*. Following leaf flush, the ε_C values of *B. occidentalis* initially continued to become less negative throughout leaf expansion phenophase (DOY 141 to 167). Following leaf flush and during leaf expansion, ε_C values from *P. angustifolia* immediately became less negative (DOY 146 to 161), while ε_C from *A. negundo* transitioned to more negative values during the same phenological stages. Following leaf expansion, the ε_H values in all species become relatively stable, corresponding to limited variation in both $\delta^{13}C_{n\text{-alkane}}$ and $\delta^{13}C_{bulk}$ values. In the mature leaves, the mean ε_C was − 5.2 ± 0.5‰ (1σ, $n = 6$), − 3.2 ± 0.3‰ (1σ, $n = 7$), and − 7.5 ± 0.6‰ (1σ, $n = 6$) for *B. occidentalis*, *P. angustifolia*, and *A. negundo*, respectively.

Discussion

Seasonal dynamics of *n*-alkane concentrations and distributions

Leaf wax *n*-alkanes and other lipids are generally considered an adaptation to reduce water loss from the leaf, to provide a photoprotective layer, and to deter pathogens (Eglinton and Hamilton 1967; Guiz 1994; Riederer and Markstadter 1996; Shepherd and Griffiths 2006). The concentrations of *n*-alkanes can be shaped by a plant's environment (Bondada et al. 1996; Riederer and Schneider 1990; Shepherd and Griffiths 2006) with the mean concentration of 506 ± 497 µg g^{-1} observed in angiosperm leaf material (Bush and McInerney 2013). Here, we found the mean concentration of *n*-alkanes to be 486 ± 510, 825 ± 342, 1064 ± 859 µg g^{-1} for *B. occidentalis*, *P. angustifolia*, and *A. negundo*, respectively (Table 1). The mean concentrations of *n*-alkanes for *B. occidentalis* were not statistically different from the average angiosperm, while both *n*-alkane concentrations for *P. angustifolia*, and *A. negundo* were significantly higher from the average angiosperm (*t*-test, $p = 0.0147$ and $p < 0.0001$, respectively). Nonetheless, concentrations of total and individual *n*-alkanes were not constant and varied throughout the study period. In general, the concentration of total *n*-alkanes dropped precipitously from the initial collection in the bud phenophase, likely due to increased mass from bud swelling (Fig. 1). During the leaf expansion phenophase, the concentration of total *n*-alkanes stabilized or slightly increased,

Table 4 Carbon isotope values of bulk foliar material and mean *n*-alkanes from the three tree species

Ordinal date	*Betula occidentalis*									*Populus angustifolia*									*Acer negundo*								
	Phenophase	$\delta^{13}C$ bulk leaf (‰, VPDB)		SD	$\delta^{13}C$ n-C_{27} (‰, VPDB)		SD	$\delta^{13}C$ n-C_{29} (‰, VPDB)		SD	Phenophase	$\delta^{13}C$ bulk leaf (‰, VPDB)		SD	$\delta^{13}C$ n-C_{27} (‰, VPDB)		SD	$\delta^{13}C$ n-C_{29} (‰, VPDB)		SD	Phenophase	$\delta^{13}C$ bulk leaf (‰, VPDB)		SD	$\delta^{13}C$ n-C_{29} (‰, VPDB)		SD	$\delta^{13}C$ n-C_{31} (‰, VPDB)		SD
112	Bud	− 28.7	±	1.0	− 31.9	±	2.0	− 31.6	±	1.6	Bud	− 31.1	±	0.9	− 35.6	±	0.9	− 34.8	±	0.8	Bud	− 27.2	±	1.3	− 33.9	±	1.1	− 33.2	±	0.7
123	Bud	− 29.2	±	1.3	− 32.7	±	2.6	− 32.6	±	2.3	Bud	− 30.8	±	1.2	− 35.6	±	1.3	− 34.5	±	1.4	Bud	− 28.4	±	1.2	− 33.3	±	1.3	− 32.7	±	1.7
132	Bud	− 28.8	±	0.8	− 33.5	±	2.4	− 33.5	±	2.4	Bud	− 31.3	±	0.5	− 36.2	±	0.6	− 35.4	±	0.5	Bud	− 28.3	±	0.8	− 33.5	±	0.6	− 32.7	±	0.5
137	Bud	− 28.0	±	0.9	− 33.1	±	1.5	− 33.1	±	1.3	Bud	− 30.9	±	1.4	− 36.0	±	1.4	− 35.5	±	1.4	Bud	− 27.7	±	0.7	− 33.3	±	1.2	− 32.6	±	1.6
141	Leaf expansion	− 28.0	±	0.8	− 33.7	±	2.0	− 33.6	±	1.9	Bud	− 30.1	±	0.3	− 36.5	±	0.1	− 36.2	±	0.2	Leaf expansion	− 28.2	±	0.7	− 33.5	±	0.7	− 32.6	±	0.5
146	Leaf expansion	− 27.9	±	0.6	− 34.1	±	0.9	− 34.6	±	1.1	Leaf expansion	− 29.5	±	1.1	− 36.5	±	0.8	− 36.5	±	0.5	Leaf expansion	− 28.3	±	1.0	− 33.8	±	1.3	− 33.0	±	1.3
153	Leaf expansion	− 28.2	±	0.6	− 32.9	±	1.8	− 32.7	±	1.8	Leaf expansion	− 29.9	±	0.7	− 36.6	±	0.5	− 36.2	±	0.6	Leaf expansion	− 28.3	±	0.7	− 34.1	±	0.7	− 33.4	±	0.6
161	Leaf expansion	− 29.4	±	0.7	− 33.6	±	1.4	− 34.4	±	1.1	Leaf expansion	− 30.3	±	0.1	− 36.0	±	1.0	− 34.1	±	1.2	Leaf expansion	− 29.6	±	1.0	− 35.1	±	1.7	− 35.1	±	1.5
167	Leaf expansion	− 30.1	±	0.9	− 35.0	±	1.5	− 34.6	±	1.0	Mature	− 31.1	±	0.4	− 36.3	±	0.1	− 34.5	±	0.5	Leaf expansion	− 29.8	±	0.6	− 36.2	±	1.2	− 36.8	±	1.1
179	Mature	− 29.9	±	0.8	− 33.5	±	1.3	− 34.1	±	1.0	Mature	− 31.1	±	0.4	− 35.9	±	0.7	− 34.3	±	0.7	Mature	− 30.1	±	0.5	− 36.3	±	1.0	− 37.0	±	1.1
195	Mature	− 30.1	±	0.9	− 34.2	±	1.7	− 34.9	±	1.4	Mature	− 31.4	±	0.7	− 36.2	±	0.8	− 34.6	±	1.0	Mature	− 30.3	±	0.6	− 36.5	±	1.2	− 37.2	±	1.7
216	Mature	− 29.8	±	0.6	− 33.9	±	0.9	− 34.9	±	0.6	Mature	− 31.2	±	0.1	− 35.8	±	0.3	− 34.4	±	0.2	Mature	− 30.2	±	0.6	− 36.7	±	0.9	− 37.4	±	0.9
239	Mature	− 29.6	±	0.7	− 33.9	±	1.1	− 35.0	±	1.2	Mature	− 31.1	±	0.2	− 35.3	±	0.6	− 34.0	±	0.1	Mature	− 29.8	±	1.1	− 36.9	±	0.5	− 37.6	±	0.7
250	Mature	− 29.3	±	1.2	− 33.5	±	1.9	− 34.7	±	1.3	Mature	− 31.1	±	0.7	− 35.2	±	1.0	− 33.8	±	0.9	Mature	− 29.8	±	1.3	− 37.5	±	0.8	− 38.0	±	0.8
274	Mature	− 29.5	±	0.6	− 33.9	±	0.8	− 35.1	±	0.4	Mature	− 31.8	±	0.8	− 36.1	±	0.6	− 34.7	±	0.6	Mature	− 30.3	±	0.8	− 36.8	±	0.7	− 36.9	±	0.8

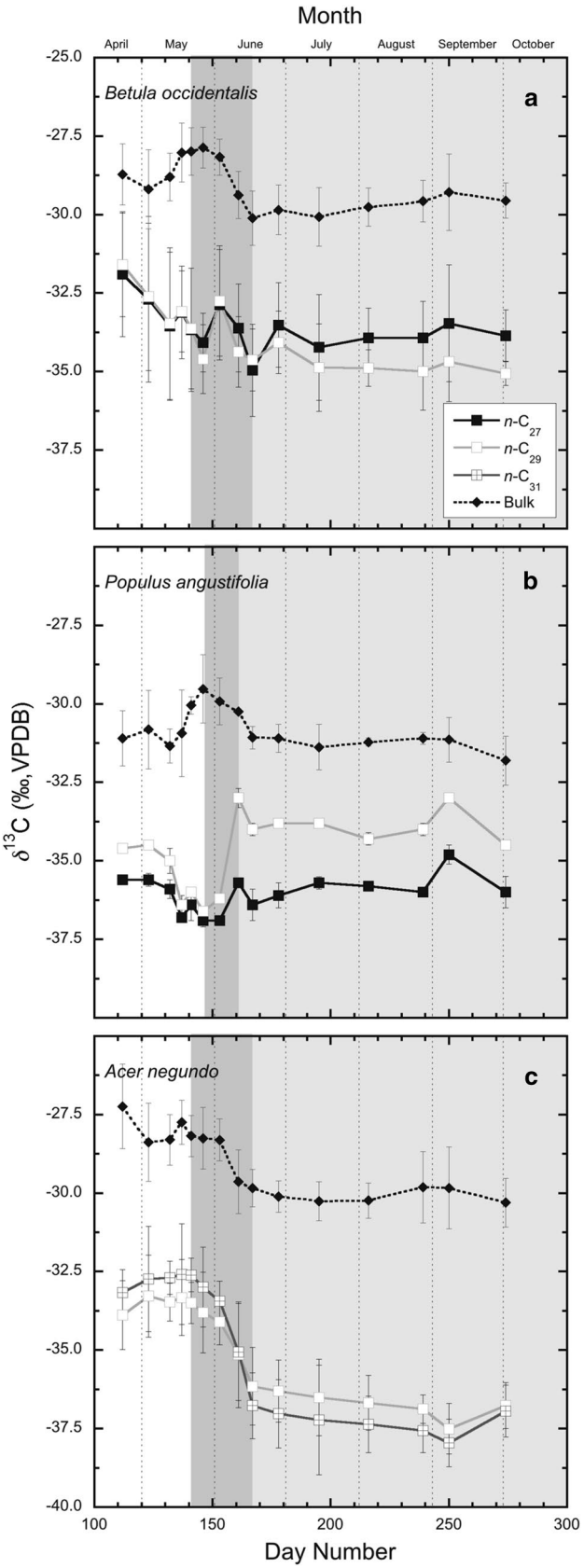

Fig. 4 Carbon isotope values of bulk leaf and *n*-alkanes from **a** *Betula occidentalis*, **b** *Populus angustifolia*, and **c** *Acer negundo*. Carbon isotope values of bulk leaf materials are shown in closed diamonds, while data from *n*-C_{27}, *n*-C_{29}, and *n*-C_{31} are shown in closed, open, and crossed squares, respectively. Error bars represent the standard deviations around the mean of the three individuals from each species used in this study. Colored areas correspond to the bud (white), leaf expansion (dark gray), and mature leaf (light gray) phenophases

suggesting lipid synthesis and production during leaf expansion. Following leaf expansion, the concentration of total *n*-alkanes stabilized or decreased in all species, pointing toward either decreased *n*-alkanes production, leaf wax ablation, or increased leaf mass from leaf thickening. We cannot distinguish among these possibilities, but note that similar seasonal dynamics in the concentration of total and individual *n*-alkanes has been previously observed in studies of broad-leaf deciduous angiosperms (Jetter and Schaffer 2001; Newberry et al. 2015; Oakes and Hren 2016; Piasentier et al. 2000; Sachse et al. 2009). After leaf flush and the initial leaf lipid formation, variations in leaf surface area likely have a significant impact on the concentration of *n*-alkanes resulting in an apparent decrease in lipid concentration (Freimuth et al. 2017). Here, a finite amount of *n*-alkane and other lipids likely were distributed across a broadening and thickening leaf, resulting in an apparent decrease in *n*-alkane concentration. Thus, it was difficult to assess if the decreases in the concentration of *n*-alkanes were a result of ablation or changes in leaf morphology (Fig. 1). Recently, Freimuth et al. (2017) related concentration to leaf area, rather than dry mass, and found that the apparent decrease in concentration was likely due to dilution of initially produced *n*-alkanes over an expanding leaf area. Thus, these data suggest that the apparent seasonal variations of *n*-alkane concentration are both a function of the initial synthesis of these compounds and changes in leaf morphology.

Odd-over-even distribution of *n*-alkanes is a characteristic of higher plant *n*-alkanes (Eglinton and Hamilton 1967). The distribution of *n*-alkanes from *B. occidentalis*, *P. angustifolia*, and *A. negundo* was broadly consistent with previous observations of the carbon preference indices (CPI) of *n*-alkanes (Bush and McInerney 2013). The mean CPI of angiosperm *n*-alkanes is 11.8 ± 12.3 (Bush and McInerney 2013). Here, we found the overall mean CPI of 21.8 ± 12.1, which was significantly different from that of an average angiosperm (*t*-test, $p < 0.0001$). Furthermore, we found significant variations in CPI relative to phenophases within the individual species (Table 1). Individually, the mean CPI for *A. negundo* was not statistically different from the average angiosperm; however, the mean CPI for *B. occidentalis* and *P. angustifolia* was significantly different from the average angiosperm (*t* test, $p < 0.0001$). The mean CPI of the mature leaf from *B. occidentalis* was 20.4 ± 3.5 and significantly different from the CPI of the bud and leaf

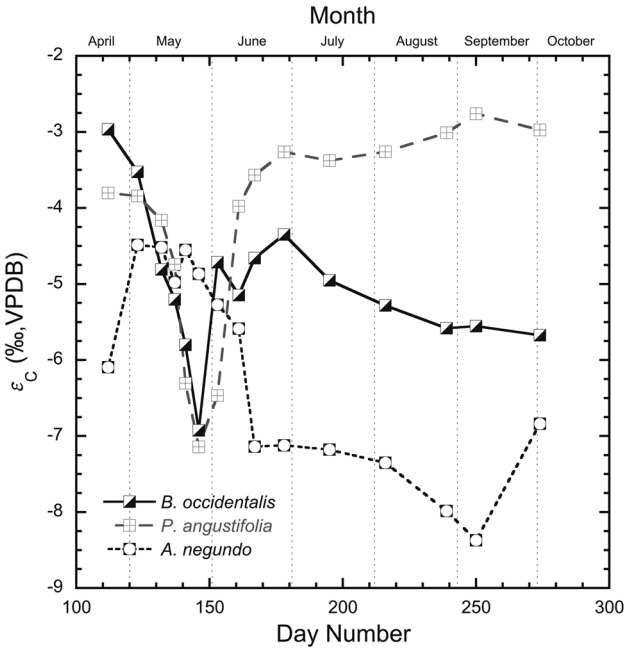

Fig. 5 Apparent fractionation between the carbon isotope values of bulk leaf material and *n*-alkanes from *Betula occidentalis*, *Populus angustifolia*, and *Acer negundo* during the studied period

expansion phenophases (37.9 ± 8.5 and 30.8 ± 9.8, respectively; *t* test, $p < 0.0001$). Furthermore, the mean CPI for each phenophase of *A. negundo* was significantly different from each other (bud: 4.6 ± 0.8, leaf expansion: 5.9 ± 0.7, mature leaf: 11.3 ± 1.3), while the mean CPI for each phenophase of *P. angustifolia* was not different from each other. CPI is an indication of the odd-over-even character of a species' *n*-alkane distribution. We observed significant variations across the growing season in two species, one of which became more strongly weighted toward odd chain lengths (e.g., *A. negundo*) and the other became less strongly weighted toward odd chain lengths (e.g., *B. occidentalis*). The distribution of *n*-alkanes on leaves has been linked to various environmental parameters (Bush and McInerney 2013; Shepherd and Griffiths 2006); however, the reasons for the removal or production of specifically odd or even *n*-alkane chain lengths following the initial formation remain abstruse.

The average chain length (ACL) of leaf waxes is a commonly applied parameter to assess the timing and variations in leaf wax development. Here, we noted systematic variations in ACL across the season corresponding to specific leaf developmental phases in all species, where the ACL values increased during leaf expansion and then stabilized (Fig. 1). Similar seasonal patterns in ACL have been observed in studies of other temperate angiosperm species (Freimuth et al. 2017; Newberry et al. 2015; Oakes and Hren 2016; Sachse et al. 2015; Tipple et al. 2013). These studies have interpreted this pattern to reflect the vast production and cessation of leaf wax development during the early ontogeny of the leaf. However, we noted that the ACL of both *P. angustifolia* and *A. negundo* stabilized following leaf expansion phenophase, while *B. occidentalis* demonstrates a more protracted transition towards stabilization during the mature leaf phenophase in the mid-summer. We observed that the three *B. occidentalis* specimens had greater variation in ACL between the individual specimens compared to *P. angustifolia* and *A. negundo* (Table S1). Studies of other angiosperm species have shown relationships between *n*-alkane distributions and environmental temperature, where higher growth temperatures were correlated with increased ACL (Bush and McInerney 2015; Maffei et al. 1993; Riederer and Schneider 1990; Sachse et al. 2006; Tipple and Pagani 2013). ACL from a variety of angiosperm species has also corresponded to plant–water relations, where drier, more water-limited conditions were correlated with increased ACL (Hughen et al. 2004; Rommerskirchen et al. 2003, 2006; Schefuss et al. 2003; Shepherd et al. 1995; Vogts et al. 2009, 2012). The distribution and composition of *n*-alkanes and other leaf waxes from specific species have been shown to be relatively plastic and adaptable to a degree, controlled largely by the plant's environmental conditions (Shepherd and Griffiths 2006). However, it is unclear how much variability in ACL could occur among individuals of the same species, growing in similar locations and environments. One possible explanation for the protracted transition to stability is that individual leaves may be experiencing slightly different microclimates. If this were the case, we would expect relatively high variability throughout the growing season. However, the ACL of the three individuals of *B. occidentalis* converged toward the end of the growing season (Fig. 1). Additionally, it may be possible that individual plants of the same species have slightly different leaf ontogenies, with specific individual plants lagging or preceding others. Further, the protracted transition may be the result of continued leaf wax production following the initial formation. However, in this scenario we would expect the δ^2H and δ^{13}C values to possibly vary in response. We will explore this hypothesis more in Sects. Interspecies differences and similarities in the δ^2H of plant waters and *n*-alkanes and Temporal trends δ^{13}C of *n*-alkanes and possible mechanisms. Nonetheless, unlike concentrations of *n*-alkanes relative to dry weight, ACL is independent of changes in leaf mass and the relatively constant ACL after leaf maturity suggests that leaf wax production largely ceases in mature leaves of broad-leaf angiosperm trees.

Interspecies differences and similarities in the δ^2H of plant waters and *n*-alkanes

Major research areas regarding the δ^2H values of leaf waxes have focused on (a) establishing the relationship between the δ^2H values of *n*-alkanes and precipitation, (b) understanding when the δ^2H signals in waxes are established, and (c) determining what are the factors controlling the δ^2H values of lipids during leaf and lipid development. Understanding the relationships between the δ^2H values of *n*-alkanes and precipitation and the timing of leaf wax formation in different plant functional types, leaf morphologies, and growth habits have been recognized as significant for geologic applications (e.g., Diefendorf and Freimuth 2017; Sachse et al. 2012). These factors, as well as, the aerial coverage, productivity, and relative concentration of leaf lipids of certain species or plant types, are important in developing robust paleo-reconstructions of plant community dynamics and hydrologic cycle variations with the isotope values of leaf wax lipids (Tipple et al. 2013). Carefully controlled natural and laboratory experiments are necessary to develop an understanding of the biological and environmental factors governing the δ^2H values of leaf waxes (Kahmen et al. 2011, 2013b; Oakes and Hren 2016; Tipple et al. 2015). These studies either control or monitor the δ^2H values of environmental water sources, as well as the δ^2H values of *n*-alkanes. As with all hydrogen within a plant's tissue, the hydrogen in *n*-alkanes is largely derived from the plant's source water and, thus, the δ^2H values of source water. The δ^2H value of source water can be altered after it enters the plant, and as the initial biosynthesis of *n*-alkanes occurs within the leaf chloroplast, the water used for synthesis can be altered due to leaf water evaporation as well as isotopic exchange with atmospheric water vapor. Several natural and controlled growth experiments have shown strong relationships between δ^2H value of leaf water and *n*-alkanes indicating that leaf water ^2H-enrichment is transferred to *n*-alkanes (Kahmen et al. 2013a, b; Tipple et al. 2015). The fractionation between biosynthetic water associated with *n*-alkane and other leaf wax lipid formation remains enigmatic and an active area of research. Biosynthetic water cannot be measured; however, leaf water is related to biosynthetic water and the δ^2H value of leaf water has often been used to estimate the biosynthetic fractionation (Freimuth et al. 2017; Gamarra et al. 2016; Kahmen et al. 2013a, b; Newberry et al. 2015; Tipple et al. 2013, 2015).

Our study site, Big Cottonwood Canyon, Utah, was specifically identified as an ideal location to conduct a semi-controlled, natural experiment where the biological and environmental factors controlling the δ^2H values of *n*-alkane ($\delta^2H_{n\text{-alkane}}$) could be isolated. At this site, the δ^2H values of stream water (δ^2H_{MW}), and most likely source water, were relatively stable throughout the growing season (Table 2), eliminating one of the main variables that control the δ^2H values of plant waters and *n*-alkanes. Plants take up soil water with no isotopic fractionation (Dawson and Ehleringer 1993) and we found that the δ^2H_{XW} values from all three species were very similar to the δ^2H_{MW} values after the cessation of leaf flush (Table 2). Nonetheless, we found that the δ^2H values of stem water (δ^2H_{XW}) diverged from the δ^2H_{MW} during the bud and leaf expansion phenophases. During these phases, the δ^2H_{XW} of all three species was less negative than the δ^2H_{MW}. Similar patterns in the δ^2H_{XW} have been observed in other broad-leaf angiosperm trees (Freimuth et al. 2017; Martin-Gomez et al. 2017; Phillips and Ehleringer 1995; Sachse et al. 2015) and have been argued to be the signature of residual evaporatively enriched xylem water from the previous winter (Phillips and Ehleringer 1995). The trend in δ^2H_{LW} corresponded to patterns in the δ^2H_{XW} during the bud and leaf expansion phenophases (Fig. 2). Following leaf expansion, the δ^2H_{LW} quickly diverged from the δ^2H_{XW} and became much less negative. The probable reason for this offset and sudden divergence is that the leaf water was affected by both evaporation and exchange with atmospheric water vapor and once the leaf was fully expanded the impact of processes was amplified. The dynamic relationship between the δ^2H_{LW}, δ^2H values of the atmospheric water vapor, and climate is well established (e.g., Dawson et al. 2002). Nonetheless, the fixed δ^2H values of the stream and xylem water after leaf expansion allow the effects of leaf water ^2H-enrichment to be highlighted.

The $\delta^2H_{n\text{-alkane}}$ from all three species also demonstrated isotopic variations corresponding to leaf developmental phenophase. We found that $\delta^2H_{n\text{-alkane}}$ from all species was lowest in the bud phenophase, became relatively ^2H-enriched throughout the leaf expansion phenophase, and stabilized after leaf expansion. These data are consistent with several previously observations of changes in $\delta^2H_{n\text{-alkane}}$ across a growing season and have been explained as the rapid de novo production of leaf waxes during the leaf flush and expansion phenophase followed by cessation of leaf wax development once the leaf was fully expanded and mature (Freimuth et al. 2017; Oakes and Hren 2016; Sachse et al. 2015; Tipple et al. 2013). Here, we found that $\delta^2H_{n\text{-alkane}}$ during the mature leaf phases was statistically different (*t* test, $p \leq 0.0096$) from one another. While both *B. occidentalis* and *A. negundo* had similar leaf phenology—leafing out during the same interval—the $\delta^2H_{n\text{-alkane}}$ from mature leaves was different. These interspecies differences could be due to different strategies for de novo synthesis, variations in H-sources, or possibly unique biosynthetic fractionations. We observed differences in the temporal expression of the δ^2H values of *n*-alkanes from *B. occidentalis* and *A. negundo*, with the $\delta^2H_{n\text{-alkane}}$ stabilizing slightly after leaf expansion in *B. occidentalis*, whereas in *A. negundo*, the $\delta^2H_{n\text{-alkane}}$ is stabilized at the initial leaf expansion (Fig. 2).

These differences may possibly be due to species-specific strategies for de novo synthesis of leaf waxes. One possible mechanism may relate to differences in ecology, where *A. negundo* are much more cosmopolitan, thriving in many environments relative to the exclusively riparian *B. occidentalis*. *A. negundo* is adapted to a wider variety of conditions, including more water-stressed environments and, as a result, *A. negundo* may develop its cuticular leaf waxes much earlier in the growing season to preempt possible variations in early season conditions. Nonetheless, the temporal expression of the $\delta^2H_{n\text{-alkane}}$ from *P. angustifolia* is similar to *A. negundo*, and *P. angustifolia* is exclusively a riparian species. These patterns may also be a response to differences in growth form, where both *P. angustifolia* and *A. negundo* are fast growing, upright tree species, while *B. occidentalis* presents a more multi-stemmed form. The $\delta^2H_{n\text{-alkane}}$ from multi-stemmed shrubs has been shown to be relatively less negative than tree species (Sachse et al. 2012)—consistent with our findings here. This pattern in shrubs has been reasoned to reflect leaf water enrichment associated with more xeric shrub habitats (Sachse et al. 2012). Although here, the site location was riparian (mesic) and the source water and environmental conditions were identical for these three species; thus, the differences in absolute $\delta^2H_{n\text{-alkane}}$ between these species must be related to additional factors.

The apparent biosynthetic fractionation between the δ^2H values of leaf water and *n*-alkane (ε_H) in all species exhibited significant variations throughout the growing season. ε_H was least negative during or immediately following the leaf expansion phenophase (Fig. 3) and was similar to those previously reported during leaf expansion (Freimuth et al. 2017; Newberry et al. 2015; Sachse et al. 2015). However, during the mature leaf phenophase, we observed ε_H values that became progressively more negative as the season progressed (Fig. 3). The overall mean ε_H during this period was $-148 \pm 27‰$ (1σ, $n = 13$). By tracing both the $\delta^2H_{n\text{-alkane}}$ and δ^2H_{LW}, it was evident that this variation was due to enrichment of ^2H in the leaf water and not changes in the $\delta^2H_{n\text{-alkane}}$ value (Fig. 2). These data suggest that in natural systems, ε_H is only meaningful during the time of leaf wax development and will fluctuate post-development due to changes in the δ^2H_{LW} of leaf water. While determining the "true" biosynthetic fractionation is not possible, greenhouse studies where the δ^2H of source water and atmospheric water vapor have been maintained throughout leaf wax develop may be the best approximation. Greenhouse studies using *B. occidentalis* and a similar *Populus* species, *P. fremontii*, found ε_H of -150 ± 9 and $-164 \pm 10‰$ for these species, respectively (Tipple et al. 2015). While both this and the greenhouse study demonstrate variability in ε_H, the mean ε_H values calculated in this study were less negative and variable, suggesting a contribution of more ^2H-enriched H-source in the field-grown plants. One difference between this study and the greenhouse study was that this study used mature trees and the greenhouse study used saplings. Potentially, the mature trees were able to utilize stored ^2H-enriched carbohydrates in leaf wax lipid production, whereas the saplings were more dependent of recent photosynthate for lipid formation. Nonetheless, this suggests that "true" biosynthetic fractionation is largely related on the δ^2H_{LW} during the period of de novo *n*-alkane synthesis and aberrations in ε_H in broad-leaf angiosperms are related to variations in δ^2H_{LW} after leaf wax formation.

Temporal trends $\delta^{13}C$ of *n*-alkanes and possible mechanisms

Carbon isotope values of plant tissues are used to track the transition from heterotrophic to autotrophic growth in plants and to assess offsets between photosynthetic and non-photosynthetic plant tissues (Cernusak et al. 2009; Dietze et al. 2014; Kimak et al. 2015; Leavitt and Long 1982, 1985; Li et al. 2007; Terwilliger 1997; Terwilliger et al. 2001). Within C_3 plants, non-photosynthetic stems, roots, fruits, and seeds, as well as emerging leaves tend to be ^{13}C-enriched relative to fully mature leaf tissue (Brugnoli and Farquhar 2000; Cernusak et al. 2002, 2007; Park and Epstein 1960). Given the importance of non-photosynthetic plant materials in paleoclimate reconstructions, such as tree ring cellulose and leaf wax *n*-alkanes, it remains a challenge to develop mechanistic understandings of these carbon isotopic offsets. However, a mechanistic understanding of the relationship between the $\delta^{13}C$ of *n*-alkanes and leaf tissues remains imperfect. Previous analyses of the $\delta^{13}C$ of *n*-alkanes across a growth period showed either little to no change or significant variations in $\delta^{13}C_{n\text{-alkane}}$ (Pedentchouk et al. 2008). Nonetheless, it is difficult to determine the underlying mechanisms for these variations as leaf developmental phenophase was not noted. Here, we compared the $\delta^{13}C$ of *n*-alkanes and leaf tissues across the growing season in relation to leaf development to assess the heterotrophic–autotrophic transition between these two materials.

Deciduous species remobilize reserve carbohydrates from previous years to initially build their photosynthetic tissues. These carbohydrates are converted into metabolic intermediates and utilized in the biosynthesis of other compounds and tissues. The $\delta^{13}C$ of emerging leaves tends to become initially less negative and then became more negative as the new leaf became photosynthetically competent. The reason for this $\delta^{13}C$ pattern in new leaves remains a subject of debate, but developmental variations in photosynthetic discrimination against ^{13}C may be a possible explanation (Cernusak et al. 2009). We found that the $\delta^{13}C$ of bulk leaf material ($\delta^{13}C_{bulk}$) was consistent with these previous studies (Fig. 4). Here, the $\delta^{13}C_{bulk}$ of these three species became less negative prior to leaf flush and then became more negative

until the leaf was fully expanded. One hypothesis that has been put forward to explain the ^{13}C-enrichment followed by ^{13}C-depletion in young leaves is that these leaves undergo a shift in the discrimination related to leaf ontogeny, where the expanding leaves have a greater discrimination against ^{13}C than mature leaves and/or the re-fixation of respired CO_2 before young leaves are capable of net CO_2 fixation (Cernusak et al. 2001, 2009; Francey et al. 1985; Terwilliger 1997; Terwilliger et al. 2001).

Where the bulk leaf material from all three species showed the expected $\delta^{13}C$ pattern from remobilization and incorporation of stored carbon into the leaf tissue, the pattern in the $\delta^{13}C$ of *n*-alkanes ($\delta^{13}C_{n\text{-alkane}}$) varied and was not consistent between the three species. We found that each species had a unique pattern in $\delta^{13}C_{n\text{-alkane}}$ during the bud and leaf expansion phenophases, suggesting the possible differences in carbon metabolism and/or biosynthesis of *n*-alkanes during the initial development of leaf waxes. The $\delta^{13}C_{n\text{-alkane}}$ from *A. negundo* showed a slight enrichment in ^{13}C during the bud phenophase (i.e., < 1‰), followed by a ~ 4‰ depletion in ^{13}C during leaf expansion (Fig. 4). While this pattern broadly mirrors that observed in the $\delta^{13}C_{bulk}$, the absolute values were different. This pattern is consistent with the current understanding of remobilization and incorporation of stored carbon from previous growth season into young leaf tissues and non-photosynthetic components, followed by the incorporation of recently fixed carbon into these materials once the leaf becomes photosynthetically competent. Similar variations across the growing season have also been observed in the $\delta^{13}C$ values of leaf cellulose of several angiosperm tree species (Kimak et al. 2015). On the other hand, both the *B. occidentalis* and *P. angustifolia* demonstrated a 1-2‰ depletion in ^{13}C during the bud phenophase, followed by a ~ 1–2‰ enrichment in ^{13}C during the leaf expansion phenophase (Fig. 4). This pattern indicates that fatty acid synthesis and elongation are decoupled from photosynthetic tissue development during this period of development. This pattern may also suggest that the carbon stock used in the production of *n*-alkyl leaf wax lipids during the early growing season may derive from a different store relative to other leaf tissues or additional isotopic branch points may exist in some species (Hayes 1993). Nonetheless, the comparison of the $\delta^{13}C_{n\text{-alkane}}$ of these three species suggests that strategies of leaf wax development may not be consistent between broad-leaf angiosperm tree species.

The apparent fractionation between the $\delta^{13}C$ values of leaf material and *n*-alkane (ε_C) in each species demonstrated significant variations related to leaf development phenophase. We observed large (i.e., > 3‰) variations in ε_C in all species during the initial growing season followed by relative stability after the leaf fully expands (Fig. 5). As with $\delta^{13}C_{n\text{-alkane}}$, the patterns in ε_C suggest a decoupling between leaf development and leaf wax formation. The transient nature of the ε_C signal may suggest the isotopic variations in both the leaf material and *n*-alkane due to variations in the stored carbon materials utilized during the initial growing season. Generally, the ε_C is calculated from the $\delta^{13}C$ values of leaf material and *n*-alkanes on fully mature leaves. The mean ε_C between $\delta^{13}C$ values of leaf material and *n*-C_{27}, *n*-C_{29}, and *n*-C_{31} alkanes for temperate angiosperm tree species is -4.6 ± 2.0‰ (Diefendorf and Freimuth 2017). Here, we found that the mean ε_C for mature leaves from the three species was unique from each other (*t* test, $p < 0.0001$), but only the ε_C from *A. negundo* was unique from the mean ε_C from temperate angiosperm tree species (*t* test, $p = 0.0006$). The ε_C value has been shown to vary among closely related tree species grown in the same environment (Diefendorf et al. 2015b). In particular, the ε_C of numerous conifer species has been related to the Family level, with these distinctions hypothesized to be related to differences in carbon storage, allocation, and metabolism (Diefendorf et al. 2015b; Freeman and Pancost 2013). While the biochemical mechanisms underlying these patterns are unknown, these data suggest that coupling the carbon isotope values of leaf materials and leaf wax lipids in controlled growth environments may be a productive method to uncover the fundamental mechanisms driving these isotopic differences and the ecological information encoded within these isotopic signals.

Coupling temporal patterns of hydrogen and carbon isotope values of *n*-alkanes

As described above, the δ^2H and $\delta^{13}C$ values of *n*-alkanes individually provide information on plant–water relations and growth environment, respectively. When both are measured in the same material, a significant relationship has been observed between δ^2H and $\delta^{13}C$ values of *n*-alkanes and other *n*-alkyl lipids within individual plants and plants using the same photosynthetic pathway (Chikaraishi and Naraoka 2003; Chikaraishi et al. 2004b; Feakins and Sessions 2010b; Pedentchouk et al. 2008). The apparent fractionations, ε_H and ε_C, have also been shown to be distinctive between photosynthetic pathways and have been suggested as a method to distinguish potential sources of *n*-alkanes and other lipids in geologic materials (Chikaraishi and Naraoka 2003; Chikaraishi et al. 2004b). These relationships have been used to interpret the $\delta^2H_{n\text{-alkane}}$ and $\delta^{13}C_{n\text{-alkane}}$ from ancient plants (Magill et al. 2013; Tipple and Pagani 2010). However, the seasonal variations in and between $\delta^2H_{n\text{-alkane}}$ and $\delta^{13}C_{n\text{-alkane}}$ are relatively unknown.

The relationship between $\delta^2H_{n\text{-alkane}}$ and $\delta^{13}C_{n\text{-alkane}}$ varied with leaf development phenophase (Fig. 6). We found relatively consistent trends in $\delta^2H_{n\text{-alkane}}$ and $\delta^{13}C_{n\text{-alkane}}$ within the bud, leaf expansion, and mature leaf phenophases. A linear trajectory was observed between the $\delta^2H_{n\text{-alkane}}$ and $\delta^{13}C_{n\text{-alkane}}$ within the bud phenophase;

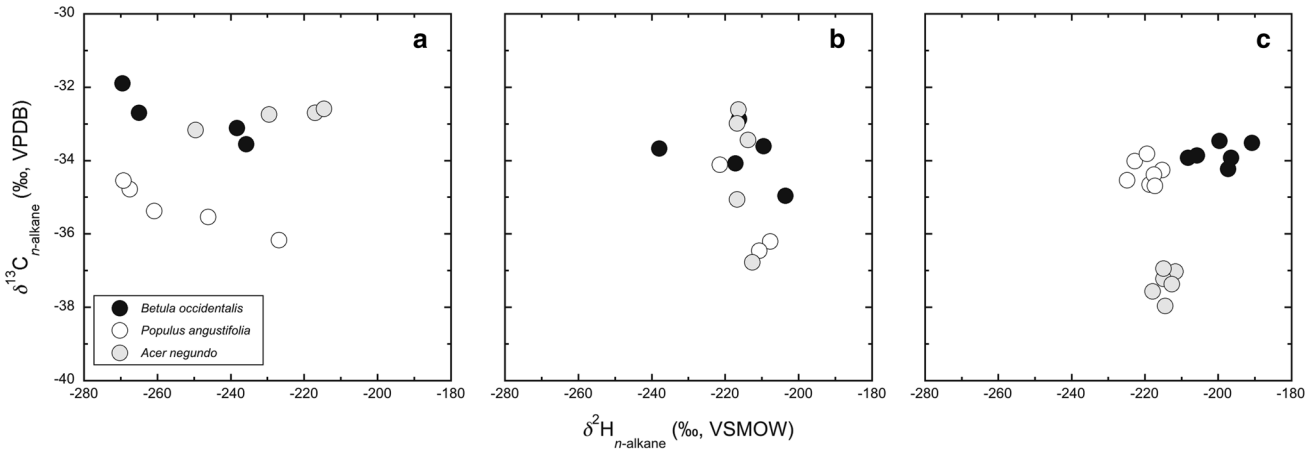

Fig. 6 Cross-plot of the carbon and hydrogen isotope values of *n*-alkanes during the **a** bud, **b** leaf expansion, and **c** mature leaf phases. Data from *Betula occidentalis*, *Populus angustifolia*, and *Acer negundo* shown in open, gray, and closed circles, respectively

however, *A. negundo* demonstrated a slight positive correspondence, while *B. occidentalis* and *P. angustifolia* showed negative correspondences. The $\delta^{2}H_{n\text{-alkane}}$ and $\delta^{13}C_{n\text{-alkane}}$ from the leaf expansion phenophase were transitory, characterized by values changing towards the values of the mature leaf phenophase (Fig. 6). As expected, the $\delta^{2}H_{n\text{-alkane}}$ and $\delta^{13}C_{n\text{-alkane}}$ from the mature leaf phenophase were relatively constant throughout the remainder of the growing season, with all three species occupying unique $\delta^{2}H_{n\text{-alkane}}/\delta^{13}C_{n\text{-alkane}}$ space.

The transition from heterotrophy to autotrophy within leaf wax production could be identified when $\delta^{2}H_{n\text{-alkane}}$ and $\delta^{13}C_{n\text{-alkane}}$ were coupled and monitored throughout the growing season. Here, we observed that the initial $\delta^{2}H_{n\text{-alkane}}$ and $\delta^{13}C_{n\text{-alkane}}$ values from buds reflected residual waxes, likely produced during the previous growing season. Once the bud became active, new *n*-alkanes were produced with a hydrogen source material that was ^{2}H-enriched relative to residual bud lipids. The carbon source material utilized to produce *n*-alkanes during this heterotrophic phase appeared to be either ^{13}C-enriched or -depleted depending on species. These data suggested that the precursors to the NADPH and pyruvate utilized in initial production of leaf wax *n*-alkanes might be variable. It remains unclear if these signals change annually or if these species continually utilize similar precursors. Once the leaf became photosynthetic active, relatively large variations in the $\delta^{2}H_{n\text{-alkane}}$ and $\delta^{13}C_{n\text{-alkane}}$ were apparent, suggesting that new photosynthate and biosynthetic water was utilized during this later leaf expansion period. Following leaf maturity, the $\delta^{2}H_{n\text{-alkane}}$ and $\delta^{13}C_{n\text{-alkane}}$ were unchanged indicating little to no new leaf wax production. Thus, the final $\delta^{2}H_{n\text{-alkane}}$ and $\delta^{13}C_{n\text{-alkane}}$ values represented a mixture of isotopic signatures from the heterotrophic and autotrophic phases of leaf wax development.

Acknowledgements This research was supported by NSF-ISO-1052551. The authors thank Bastian Hambach, Christine Doman, and Susanna Khachaturyan for their assistance in the analysis of the carbon isotope values of leaf waxes, hydrogen isotope values of leaf waxes, and hydrogen isotope ratios of plant and environmental waters, respectively. The authors also wish to thank Katherine H. Freeman and Ansgar Kahmen for helpful insights and discussions that strengthened this contribution.

Author contribution statement BJT and JRE conceived and designed experiment. BJT performed the experiment and analyzed the data. BJT and JRE wrote the manuscript.

References

Alstad KP, Hart SC, Horton JL, Kolb TE (2008) Application of tree-ring isotopic analyses to reconstruct historical water use of riparian trees. Ecol Appl 18:421–437

Berke MA, Johnson TC, Werne JP, Schouten S, Sinninghe Damste JS (2012) A mid-Holocene thermal maximum at the end of the African Humid Period. Earth Planet Sci Lett 351–352:95–104

Berke MA, Tipple BJ, Hambach B, Ehleringer JR (2015) Life form-specific gradients in compound-specific hydrogen isotope ratios of modern leaf waxes along a North American Monsoonal transect. Oecologia 179:981–997. https://doi.org/10.1007/s00442-015-3432-1

Bondada BR, Oosterhuis BM, Murphy JB, Kim KS (1996) Effect of water stress on the epicuticular wax composition and ultrastructure of cotton (*Gossypium hirsutum* L.) leaf, bract and boll. Environ Exp Bot 36:61–69

Brugnoli E, Farquhar GD (2000) Photosynthetic fractionation of carbon isotopes. In: Leegood RC, Sharkey TC, von Caemmerer S (eds) Photosynthesis: physiology and metabolism. Kluwer, Dordrecht, pp 399–434

Bush RT, McInerney FA (2013) Leaf wax *n*-alkane distributions in and across modern plants: implications for paleoecology and chemotaxonomy. Geochim Cosmochim Acta 117:161–179

Bush RT, McInerney FA (2015) Influence of temperature and C_4 abundance on *n*-alkane chain length distributions across the central USA. Org Geochem 79:65–73

Cerling TE, Quade J, Wang Y (1994) Expansion and emergence of C_4 plants. Nature 371:112–113

Cernusak LA, Marshall JD, Comer JB, Balster NJ (2001) Carbon isotope discrimination in photosynthetic bark. Oecologia 128:24–35

Cernusak LA, Pate JS, Farquhar GD (2002) Diurnal variation in the stable isotope composition of water and dry matter in fruiting *Lupinus angustifolius* under field conditions. Plant, Cell Environ 25:893–907

Cernusak LA, Aranda J, Marshall JD, Winter K (2007) Large variation in whole-plant water-use efficiency among tropical tree species. New Phytol 173:294–305. https://doi.org/10.1111/j.1469-8137.2006.01913.x

Cernusak LA et al (2009) Why are non-photosythetic tissues generally ^{13}C enriched compared with leaves in C_3 plants? Review and synthesis of current hypotheses. Funct Plant Biol 36:199–213

Chikaraishi Y, Naraoka H (2003) Compound-specific δD-$\delta^{13}C$ analyses of n-alkanes extracted from terrestrial and aquatic plants. Phytochemistry 63:361–371

Chikaraishi Y, Naraoka H (2007) $\delta^{13}C$ and δD relationships among three *n*-alkyl compound classes (*n*-alkanoic acid, *n*-alkane and *n*-alkanol) of terrestrial higher plants. Org Geochem 38:198–215

Chikaraishi Y, Naraoka H, Poulson SR (2004a) Carbon and hydrogen isotopic fractionation during lipid biosynthesis in a higher plant (*Cryptomeria japonica*). Phytochemistry 65:323–330

Chikaraishi Y, Naraoka H, Poulson SR (2004b) Hydrogen and carbon isotopic fractionations of lipid biosynthesis among terrestrial (C_3, C_4 and CAM) and aquatic plants. Phytochemistry 65:1369–1381

Choi W-J, Chang SX, Allen HL, Kelting DL, Ro H-M (2005) Irrigation and fertilization effects on foliar and soil carbon and nitrogen isotope ratios in a loblolly pine stand. For Ecol Manage 213:90–101. https://doi.org/10.1016/j.foreco.2005.03.016

Cormier M-A, Werner RA, Sauer PE, Grocke DR, Leuenberger MC, Wieloch, T, Schleucher J, Kahmen A (2018) ^2H-fractionations during the biosynthesis of carbohydrates and lipids imprint a metabolic signal on the δ^2H values of plant organic compounds. New Phytologist 218:479–491. https://doi.org/10.1111/nph.15016

Cook ER, Anchukaitis KJ, Buckley BM, D'Arrigo RD, Jacoby GC, Wright WE (2010) Asian monsoon failure and megadrought during the Last Millennium. Science 328:486–489

Dawson TE, Ehleringer JR (1991) Streamside trees that do not use stream water. Nature 350:335–337

Dawson TE, Ehleringer JR (1993) Isotopic enrichment of water in the "woody" tissue of plants: Implications for plant water source, water uptake, and other studies which use the stable isotopic composition of cellulose. Geochim Cosmochim Acta 57:3487–3492

Dawson TE, Mambelli S, Plamboeck AH, Templer PH, Tu KP (2002) Stable isotopes in plant ecology. Annu Rev Ecol Syst 33:507–559. https://doi.org/10.1146/annurev.ecolsys.33.020602.095451

Diefendorf AF, Freimuth EJ (2017) Extracting the most from terrestrial plant-derived *n*-alkyl lipids and their carbon isotopes from the sedimentary record: a review. Org Geochem 103:1–21. https://doi.org/10.1016/j.orggeochem.2016.10.016

Diefendorf AF, Freeman KH, Wing SL, Currano ED, Mueller KE (2015a) Paleogene plants fractionated carbon isotopes similar to modern plants. Earth Planet Sci Lett 429:33–44. https://doi.org/10.1016/j.epsl.2015.07.029

Diefendorf AF, Leslie AB, Wing SL (2015b) Leaf wax composition and carbon isotopes vary among major conifer groups. Geochim Cosmochim Acta 170:145–156. https://doi.org/10.1016/j.gca.2015.08.018

Dietze MC et al (2014) Nonstructural carbon in woody plants. Annu Rev Plant Biol 65:667–687. https://doi.org/10.1146/annurev-arplant-050213-040054

Douglas PM et al (2015) Drought, agricultural adaptation, and sociopolitical collapse in the Maya Lowlands. Proc Natl Acad Sci USA 112:5607–5612. https://doi.org/10.1073/pnas.1419133112

Eglinton G, Hamilton RJ (1967) Leaf epicuticular waxes. Science 156:1322–1335

Ehleringer JR, Field CB, Z-f Lin, C-y Kuo (1986) Leaf carbon isotope and mineral composition in subtropical plants along an irradiance cline. Oecologia 70:520–526

Farquhar GD, Ehleringer JR, Hubick KT (1989) Carbon isotope discrimination and photosynthesis. Ann Rev Plant Physiol Mol Biol 40:503–537

Feakins SJ, Sessions AL (2010a) Controls on the D/H ratios of plant leaf waxes from an arid ecosystem. Geochim Cosmochim Acta 74:2128–2141

Feakins SJ, Sessions AL (2010b) Crassulacean acid metabolism influences D/H ratio of leaf wax in succulent plants. Org Geochem 41:1269–1276

Flanagan LB, Comstock JP, Ehleringer JR (1991) Comparison of modeled and observed environmental influences on the stable oxygen and hydrogen isotope composition of leaf water in *Phaseolus vulgaris* L. Plant Physiol 96:588–596

Francey RJ, Gifford RM, Sharkey TD, Weir B (1985) Physiological influences on carbon isotope discrimination in huon pine (*Lagarostrobos franklinii*). Oecologia 66:211–218

Freeman KH, Colarusso LA (2001) Molecular and isotopic records of C_4 grassland expansion in the late Miocene. Geochim Cosmochim Acta 65:1439–1454

Freeman KH, Pancost RD (2013) Biomarkers for terrestrial plants and climate. In: Turekian KK, Holland HD (eds) Treatise on geochemistry. Elsevier, Second edn, pp 395–416

Freimuth EJ, Diefendorf AF, Lowell TV (2017) Hydrogen isotopes of *n*-alkanes and *n*-alkanoic acids as tracers of precipitation in a temperate forest and implications for paleorecords. Geochim Cosmochim Acta 206:166–183. https://doi.org/10.1016/j.gca.2017.02.027

Gamarra B, Kahmen A (2015) Concentrations and δ2H values of cuticular n-alkanes vary significantly among plant organs, species and habitats in grasses from an alpine and a temperate European grassland. Oecologia 178:981–998. https://doi.org/10.1007/s00442-015-3278-6

Gamarra B, Sachse D, Kahmen A (2016) Effects of leaf water evaporative ^2H-enrichment and biosynthetic fractionation on leaf wax *n*-alkane δ^2H values in C_3 and C_4 grasses. Plant, Cell Environ 39:2390–2403. https://doi.org/10.1111/pce.12789

Gessler A, Brandes E, Buchmann N, Helle G, Rennenberg H, Barnard RL (2009) Tracing carbon and oxygen isotope signals from newly assimilated sugars in the leaves to the tree-ring archive. Plant, Cell Environ 32:780–795

Griffin D, Anchukaitis KJ (2014) How unusual is the 2012-2014 California drought? Geophys Res Lett 41:9017–9023. https://doi.org/10.1002/2014gl062433

Guiz PG (1994) Epicuticular leaf waxes in the evolution of the plant kingdom. J Plant Physiol 143:453–464

Hayes JM (1993) Factors contolling ^{13}C contents of sedimentary organic compounds: Principles and evidence. Mar Geol 113:111–125

Hayes JM (2001) Fractionation of carbon and hydrogen isotopes in biosynthetic processes. Rev Mineral Geochem 43:225–253

Helliker BR, Ehleringer JR (2002) Differential ^{18}O enrichment of leaf cellulose in C_3 versus C_4 grasses. Funct Plant Biol 29:435–442

Helliker BR, Roden JS, Cook CS, Ehleringer JR (2002) A rapid and precise method for sampling and determining the isotope ratio

of atmospheric water vapor. Rapid Commun Mass Spectrom 16:929–932
Hobbie EA et al (2017) Long-term carbon and nitrogen dynamics at SPRUCE revealed through stable isotopes in peat profiles. Biogeosciences 14:2481–2494
Hughen KA, Eglinton TI, Xu L, Makou M (2004) Abrupt tropical vegetation response to rapid climate changes. Science 304:1955–1959
Jetter R, Schaffer S (2001) Chemical composition of the *Prunus laurocerasus* leaf surface. Dynamic changes of the epicuticular wax film during leaf development. Plant Physiol 126:1725–1737
Kahmen A, Dawson TE, Vieth A, Sachse D (2011) Leaf wax *n*-alkane δD values are determined early in the ontogeny of *Populus trichocarpa* leaves when grown under controlled environmental conditions. Plant, Cell Environ 34:1639–1651
Kahmen A et al (2013a) Leaf water deuterium enrichment shapes leaf wax *n*-alkane δD values of angiosperm plants II: observational evidence and global implications. Geochim Cosmochim Acta 111:50–63
Kahmen A, Schefuss E, Sachse D (2013b) Leaf water deuterium enrichment shapes leaf wax *n*-alkane δD values of angiosperm plants I: experimental evidence and mechanistic insights. Geochim Cosmochim Acta 111:39–49
Kimak A, Kern Z, Leuenberger M (2015) Qualitative distinction of autotrophic and heterotrophic processes at the leaf level by means of triple stable isotope (C–O–H) patterns. Front Plant Sci 6:1008. https://doi.org/10.3389/fpls.2015.01008
Ladd SN, Sachs JP (2017) 2H/1H fractionation in lipids of the mangrove Bruguiera gymnorhiza increases with salinity in marine lakes of Palau. Geochim Cosmochim Acta 204:300–312
Leavitt SW (2010) Tree-ring C–H–O isotope variability and sampling. Sci Total Environ 408:5244–5253
Leavitt SW, Long A (1982) Evidence for $^{13}C/^{12}C$ fractionation between tree leaves and wood. Nature 298:742–744
Leavitt SW, Long A (1985) Stable carbon isotopic composition of maple sap and foliage. Plant Physiol 78:427–429
Leavitt SW et al (2011) The North American monsoon in the U.S. Southwest: potential for investigation with tree-ring carbon isotopes. Quatern Int 235:101–107
Lee H, Feakins SJ, Sternberg LdSL (2016) Carbon and hydrogen isotopic effects of stomatal density in *Arabidopsis thaliana*. Geochim Cosmochim Acta 179:275–286. https://doi.org/10.1016/j.gca.2016.01.029
Li SG, Tsujimura M, Sugimoto A, Davaa G, Oyunbaatar D, Sugita M (2007) Temporal variation of $\delta^{13}C$ of larch leaves from a montane boreal forest in Mongolia. Trees Struct Fun 21:479–490
Liddy HM, Feakins SJ, Tierney JE (2016) Cooling and drying in northeast Africa across the Pliocene. Earth Planet Sci Lett 449:430–438. https://doi.org/10.1016/j.epsl.2016.05.005
Maffei M, Mucciarelli M, Scannerini S (1993) Environmental factors affecting the lipid metabolism in *Rosmarinus officinalis* L. Biochem Syst Ecol 21:765–784
Magill CR, Ashley GM, Freeman KH (2013) Water, plants and early human habitats in eastern Africa. Proc Natl Acad Sci 110:1167–1174
Mallette JR, Casale JF, Jones LM, Morello DR (2017) The isotopic fractionation of carbon, nitrogen, hydrogen, and oxygen during illicit production of cocaine base in South America. Forensic Sci Int 270:255–260
Martin-Gomez P, Serrano L, Ferrio JP (2017) Short-term dynamics of evaporative enrichment of xylem water in woody stems: implications for ecohydrology. Tree Physiol 37:511–522. https://doi.org/10.1093/treephys/tpw115
Marzi R, Torkelson BE, Olson RK (1993) A revised carbon preference index. Org Geochem 20:1303–1306
McCarroll D, Loader NJ (2004) Stable isotopes in tree rings. Quatern Sci Rev 23:771–801
Monson KD, Hayes JM (1980) Biosynthetic control of the natural abundance of carbon 13 at specific positions within fatty acids in *Escherichia coli*. J Biol Chem 255:11435–11441
Nasholm T, Ekblad A, Nordin A, Giesler R, Hogberg M, Hogberg P (1998) Boreal forest plants take up organic nitrogen. Nature 392:914–916
Newberry SL, Kahmen A, Dennis P, Grant A (2015) *n*-Alkane biosynthetic hydrogen isotope fractionation is not constant throughout the growing season in the riparian tree *Salix viminalis*. Geochim Cosmochim Acta 165:75–85. https://doi.org/10.1016/j.gca.2015.05.001
Oakes AM, Hren MT (2016) Temporal variations in the δD of leaf *n*-alkanes from four riparian plant species. Org Geochem 97:122–130. https://doi.org/10.1016/j.orggeochem.2016.03.010
Park R, Epstein S (1960) Carbon isotope fraction during photosynthesis. Geochim Cosmochim Acta 21:110–126
Pedentchouk N, Sumner W, Tipple BJ, Pagani M (2008) $\delta^{13}C$ and δD compositions of *n*-alkanes from modern angiosperms and conifers: an experimental set up in central Washington State, USA. Org Geochem 39:1066–1071
Phillips SL, Ehleringer JR (1995) Limited uptake of summer precipitation by bigtooth maple (*Acer gradidentatum* Nutt) and Gambel's oak (*Quercus gambelii* Nutt). Trees 9:214–219
Piasentier E, Bovolenta S, Malossini F (2000) The *n*-alkane concentrations in buds and leaves of browsed broadleaf trees. J Agric Sci 135:311–320
Riederer M, Markstadter C (1996) Cuticular waxes: a critical assessment of current knowledge. In: Kersteins G (ed) Plant cuticles: an integrated functional approach. BIOS Scientific Publishers, Oxford, pp 189–200
Riederer M, Schneider G (1990) The effect of the environment on the permeability and composition of Citrus leaf cuticle. Planta 180:154–165
Roden JS, Ehleringer JR (1999) Hydrogen and oxygen isotope ratios of tree-ring cellulose for riparian trees grown long-term under hydroponically controlled environments. Oecologia 121:467–477
Roden JS, Ehleringer JR (2000) There is no temperature dependence of net biochemical fractionation of hydrogen and oxygen isotopes in tree-ring cellulose. Isot Environ Health Stud 36:303–317
Rommerskirchen F, Eglinton G, Dupont L, Guntner U, Wenzel C, Rullkotter J (2003) A north to south transect of Holocene southeast Atlantic continental margin sediments: relationship between aerosol transport and compound-specific $\delta^{13}C$ land plant biomarker and pollen records. Geochem Geophys Geosyst 4:1101
Rommerskirchen F, Plader A, Eglinton G, Chikaraishi Y, Rullkotter J (2006) Chemotaxonomic significance of distribution and stable carbon isotopic composition of long-chain alkanes and alkan-1-ols in C_4 grass waxes. Org Geochem 37:1303–1332
Rundel PW, Ehleringer JR, Nagy KA (1989) Stable isotopes in ecological research. Springer, New York
Sachse D, Radke J, Gleixner G (2006) dD values of individual n-alkanes from terrestrial plants along a climatic gradient—implications for the sedimentary biomarker record. Org Geochem 37:469–483
Sachse D, Kahmen A, Gleixner G (2009) Significant seasonal variation in the hydrogen isotopic composition of leaf-wax lipids for two deciduous tree ecosystems (*Fagus sylvativa* and *Acer pseudoplatanus*). Org Geochem 40:732–742
Sachse D, Gleixner G, Wilkes H, Kahmen A (2010) Leaf wax *n*-alkane δD values of field-grown barley reflect leaf water δD values at the time of leaf formation. Geochim Cosmochim Acta 74:6741–6750
Sachse D et al (2012) Molecular paleohydrology: interpreting the hydrogen-isotopic composition of lipid biomarkers from photosynthesizing organisms. Annu Rev Earth Planet Sci 40:221–249
Sachse D, Dawson TE, Kahmen A (2015) Seasonal variation of leaf wax *n*-alkane production and δ^2H values from the evergreen oak

tree, *Quercus agrifolia*. Isot Environ Health Stud 51:124–142. https://doi.org/10.1080/10256016.2015.1011636
Schefuss E, Ratmeyer V, Stuut JBW, Jansen JHF, Sinninghe Damste JS (2003) Carbon isotope analyses of n-alkanes in dust from the lower atmosphere over the central eastern Atlantic. Geochim Cosmochim Acta 67:1757–1767
Schmidt H-L, Werner RA, Eisenreich W (2003) Systematics of 2H patterns in natural compounds and its importance for the elucidation of biosynthetic pathways. Phytochem Rev 2:61–85
Shepherd T, Griffiths DW (2006) The effects of stress on plant cuticular waxes. New Phytol 171:469–499
Shepherd T, Robertson GW, Griffiths DW, Birch ANE, Duncan G (1995) Effects of environment on the composition of epicuticular wax from kale and swede. Phytochemistry 40:407–417
Smith FA, Wing SL, Freeman KH (2007) Magnitude of the carbon isotope excursion at the Paleocene-Eocene thermal maximum: the role of plant community change. Earth Planet Sci Lett 262:50–65
Sparks JP, Ehleringer JR (1997) Leaf carbon isotope discrimination and nitrogen content for riparian trees along elevational transects. Oecologia 109:362–367
Szejner P et al (2016) Latitudinal gradients in tree-ring stable carbon and oxygen isotopes reveal differential climate influences of the North American monsoon system. J Geophys Res Biogeosci 121:1979–1991. https://doi.org/10.1002/2016JG003460
Terwilliger VJ (1997) Changes in the d13C values of trees during a tropical rainy season: some effects in addition to diffusion and carboxylation by Rubisco? Am J Bot 84:1693–1700
Terwilliger VJ, Kitajima K, Le Roux-Swarthout DJ, Mulkey S, Wright SJ (2001) Intrinsic water-use efficiency and hterotrophic investment in tropical leaf growth of two Neotropical pioneer tree species as estimated from $\delta^{13}C$ values. New Phytol 152:267–281
Tierney JE, Smerdon JE, Anchukaitis KJ, Seager R (2013) Multidecadal variability in East African hydroclimate controlled by the Indian Ocean. Nature 493:389–392
Tipple BJ (2013) Capturing climate variability during our ancestors' earliest days. Proc Natl Acad Sci USA 110:1144–1145
Tipple BJ, Pagani M (2010) A 35 Myr North American leaf-wax compound-specific carbon and hydrogen isotope record: implications for C_4 grasslands and hydrologic cycle dynamics. Earth Planet Sci Lett 299:250–262
Tipple BJ, Pagani M (2013) Environmental control on eastern broadleaf forest species' leaf wax distributions and D/H ratios. Geochim Cosmochim Acta 111:64–77. https://doi.org/10.1016/j.gca.2012.10.042
Tipple BJ et al (2011) Coupled high-resolution marine and terrestrial records of carbon and hydrologic cycles variations during the Paleocene-Eocene Thermal Maximum (PETM). Earth Planet Sci Lett 311:82–92
Tipple BJ, Berke MA, Doman CE, Khachaturyan S, Ehleringer JR (2013) Leaf *n*-alkane record the plant-water environment at leaf flush. Proc Natl Acad Sci 110:2659–2664
Tipple BJ, Berke MA, Hambach B, Roden JS, Ehleringer JR (2015) Predicting leaf wax *n*-alkane $^2H/^1H$ ratios: controlled water source and humidity experiments with hydroponically grown trees confirm predictions of Craig-Gordon model. Plant, Cell Environ 38:1035–1047. https://doi.org/10.1111/pce.12457
Tipple BJ, Hambach B, Barnette JE, Chesson LA, Ehleringer JR (2016) The influences of cultivation setting on inflorescence lipid distributions, concentrations, and carbon isotope ratios of *Cannabis* sp. Forensic Sci Int 262:233–241. https://doi.org/10.1016/j.forsciint.2016.03.029
Treydte KS, Frank DC, Saurer M, Helle G, Schleser GH, Esper J (2009) Impact of climate and CO_2 on a millennium-long tree-ring carbon isotope record. Geochim Cosmochim Acta 73:4635–4647
Uno KT, Polissar PJ, Jackson KE, deMenocal PB (2016) Neogene biomarker record of vegetation change in eastern Africa. Proc Natl Acad Sci 113:6355–6363. https://doi.org/10.1073/pnas.1521267113
Voelker SL et al (2016) A dynamic leaf gas-exchange strategy is conserved in woody plants under changing ambient CO_2: evidence from carbon isotope discrimination in paleo and CO_2 enrichment studies. Glob Change Biol 22:889–902
Vogts A, Moossen H, Rommerskirchen F, Rullkotter J (2009) Distribution patterns and stable carbon isotopic composition of alkanes and alkan-1-ols from plant waxes of African rain forest and savanna C_3 species. Org Geochem 40:1037–1054
Vogts A, Schefuss E, Badewien T, Rullkotter J (2012) *n*-Alkane parameters from a deep sea sediment transect off southwest Africa reflect continental vegetation and climate conditions. Org Geochem 47:109–119
West AG, Patrickson SJ, Ehleringer JR (2006) Water extraction times for plant and soil materials used in stable isotope analysis. Rapid Commun Mass Spectrom 20:1317–1321
Zhang X et al (2017) Hydrogen isotope ratios of terrestrial leaf wax *n*-alkanes from the Tibetan Plateau: controls on apparent enrichment factors, effect of vapor sources and implication for altimetry. Geochim Cosmochim Acta 211:10–27. https://doi.org/10.1016/j.gca.2017.04.035
Zhou Y et al (2010) Biosynthetic origin of the saw-toothed profile in $\delta^{13}C$ and δ^2H of n-alkanes and systematic isotopic differences between *n*-, iso- and anteiso-alkanes in leaf waxes of land plants. Phytochemistry 71:388–403. https://doi.org/10.1016/j.phytochem.2009.11.009
Zhou Y, Grice K, Stuart-Williams H, Hocart CH, Gessler A, Farquhar GD (2016) Hydrogen isotopic differences between C_3 and C_4 land plant lipids: consequences of compartmentation in C_4 photosynthetic chemistry and C_3 photorespiration. Plant, Cell Environ 39:2676–2690. https://doi.org/10.1111/pce.12821
Zimmerman J, Ehleringer JR (1990) Carbon isotope ratios are correlated with irradiance levels in the Panamanian orchid *Catasetum viridiflavum*. Oecologia 83:247–249